# Calibration Results of the NASA Ames Rotor Test Apparatus Steady/Dynamic Rotor Balance

Johannes M. van Aken*
Sterling Software
NASA Ames Research Center
Moffett Field, California

Randall L. Peterson**
NASA Ames Research Center
Moffett Field, California

Cynthia J. Freedman***
Sterling Federal Systems
Sterling Software
Palo Alto, California

## Abstract

The NASA Ames Rotor Test Apparatus was recently modified to include a steady/dynamic rotor balance. The calibration procedures and data reduction process to obtain static and dynamic calibration coefficients are discussed. Verification of the dynamic calibration procedures and the data processing for the low frequency range was accomplished by means of a hub imbalance run. Representative results of the balance predictions for the hub imbalance forces and moments are provided.

## Nomenclature

| | |
|---|---|
| n | integer per rev harmonic, n=1,2,... |
| NF | normal force, positive up, lb |
| NFi | normal force on flexure i, positive up, lb |
| PM | pitch moment, positive nose up, ft-lb |
| RM | roll moment, positive right wing down, ft-lb |
| AF | axial force, positive aft, lb |
| SF | side force, positive to right, lb |
| $V_X$ | output voltage for strain gage X, mV |
| $\alpha$ | model angle of attack, deg |

## Introduction

Accurate measurements of the vibratory loading of a rotor system have long been a challenge to the rotorcraft community (Refs. 1-4). In 1987, NASA Ames identified the requirement to extend the capability of the Rotor Test Apparatus (RTA) to measure both the steady and vibratory hub forces and moments to thrust levels of 22,000 lb. From this requirement a rotor balance was designed, fabricated, and calibrated to measure both the steady and vibratory thrust, torque, shears, and moments of any rotor system installed on the RTA.

This paper first describes the Rotor Test Apparatus and the Steady/Dynamic Rotor balance. Subsequently the static balance calibration method and its results will be discussed. Next the dynamic balance calibration procedure and representative results thereof will be presented. Verification results of the dynamic calibration at low frequencies will be presented using the data from a hub imbalance run for a representative rotor system. Finally, recommendations are made for further investigations of the balance dynamic response characteristics, which might lead to improvements in the balance dynamic load predictions.

## Test Hardware

### Rotor Test Apparatus

The NASA Ames Rotor Test Apparatus (RTA) is a special-purpose drive and support system for operating helicopter rotors in the 40- by 80- and 80- by 120-Foot Wind Tunnels. The RTA houses two electric drive motors, the hydraulic servo-actuators of the primary control-system, and a dynamic control system capable of introducing dynamic perturbations to the non-rotating swashplate (collective and tilt) at frequencies up to 40 Hz. Recent modifications to the RTA include the addition of a five-component balance to measure rotor loads at the hub moment center. This balance was designed and fabricated to measure both the steady and vibratory rotor normal, axial, and side forces, together with rotor pitch and roll moments to rotor thrust levels of 22,000 lb. The balance

*Research Engineer.
**Aerospace Engineer.
***Program Analyst.

Presented at the American Helicopter Society Aeromechanics Specialists Conference, San Francisco, California, January 19-21, 1994. 

natural frequencies are all above 60 Hz. An instrumented flex-coupling measures rotor torque and residual thrust.

**Steady/Dynamic Rotor Balance**

The five-component Steady/Dynamic Rotor Balance (S/DRB) is located between the RTA transmission and upper housing. It consists of two rings with a 28-in inner diameter and a 32-in outer diameter, which are connected to each other by four rectangular, instrumented flexures. The centers of the four flexures are located on a 30-in diameter circle.

Figure 1 shows a schematic top view of the five-component ring balance. The flexures are identified by the numbers 1 through 4. Flexures 1 and 2 are located in the longitudinal plane in the aft and forward locations, respectively. Flexures 3 and 4 are located in the lateral plane at the right and left positions, respectively. The balance flexures are 2.872 in tall and have a rectangular cross-section measuring 0.540- by 1.068-in. The flexures are oriented such that the long side of the rectangular cross section is tangential to the balance circumference. Figure 2 shows the balance. The balance was retrofitted to the existing RTA model and installed on top of the RTA transmission. The presence of an extrusion to accommodate the transmission idler shaft and bearing resulted in a large cutout in the non-metric side of the balance. This 45 deg pie shape cutout is clearly visible in Fig. 2 in the lower left side of the balance. The cutout is located directly under flexure 1 and resulted in some large balance gage interactions.

The balance peak load capacities are: 22,000 lb of thrust, 4,400 lb of resultant shear force, and 57,800 ft-lb of resultant moment at the balance moment center. The maximum allowable resultant hub moment depends upon the hub height above the balance moment center. The balance shares a common centerline with the rotor shaft. The rotor shaft has an in-line flex-coupling, which is instrumented to measure rotor torque up to a maximum of 36,000 ft-lb and the residual shaft thrust up to a calibration limit of 200 lb.

The vibratory load capabilities of the balance are: 5,500 lb of thrust, 1,100 lb of resultant shear force, and 8,920 ft-lb of resultant moment.

**Balance Gauging**

Each of the four flexures is instrumented with a four-arm active Wheatstone bridge to measure loading in the flexure axial direction (balance normal force direction). These four individual normal force component readings, $V_{NFi}$, i=1-4, can be summed to provide the balance normal force reading, $V_{NF}$; $V_{NF}=V_{NF1}+V_{NF2}+V_{NF3}+V_{NF4}$. The readings from the opposing flexures can be differenced to provide pitch and roll moment readings; $V_{PM}=V_{NF1}-V_{NF2}$ and $V_{RM}=V_{NF3}-V_{NF4}$, respectively.

Each of the four flexures is also instrumented with a four-arm active Wheatstone bending bridge, measuring the shear force along the long side of the flexure cross-section. The strain gage outputs of opposing flexures are wired into a Wheatstone bridge so as to provide the balance axial force reading, $V_{AF}$ (from flexures 3 and 4), and the balance side force reading, $V_{SF}$ (from flexures 1 and 2).

**Balance Monitoring**

The balance provides six gage readings, being NF1, NF2, NF3, NF4, AF, and SF. The summing and differencing of the NFi gages into the NF, PM, and RM readings are done digitally in the balance data reduction program.

A Balance Analog Monitoring Box (BAMB) is used for on-line monitoring to ensure safe operation of the rotor system and the balance. This box combines the six balance gage outputs into analog signals representing the various forces and moments in both the balance- and the hub-axis systems. This on-line analog process does not provide for balance gage interaction corrections. The various analog output signals from the BAMB are displayed on an analog bar chart monitor or on an oscilloscope to perform the on-line safety-of-flight monitoring during actual wind tunnel testing.

The BAMB analog signals for NF, PM, and RM were also acquired during the shake test for use in determining the dynamic calibration matrix. Subsequently these signals were acquired in the imbalanced hub tests. Data from these tests were used in evaluating the accuracy of the dynamic load measurements.

**Installed Static Balance Calibration**

Various attempts were made to perform an accurate bench calibration of the balance. It was found, however, that the balance boundary conditions and load paths as seen by the balance in the RTA installation could not be reproduced in the laboratory calibration test rig. This resulted in considerable errors in the balance gage interaction readings. An RTA installed balance calibration was therefore performed.

The S/DRB was installed into the RTA. A calibration fixture, resembling the upper housing geometry, was installed onto the balance. This fixture allowed for the application of balance axial, side, and normal forces through the balance moment center. Balance moments were applied by off-center loading of normal force, thus exerting both a normal force and moment onto the balance. The calibration fixture allowed for the installation of weight baskets to preload the balance in the normal force direction by the weight of both the upper housing assembly and a typical helicopter rotor system. The RTA was then placed in a special calibration test rig (Fig. 3). Hydraulic actuators, installed between the calibration fixture and the calibration test rig, were used to apply the static calibration loading. In-line load cells measured the load applied by these actuators. Knowledge of the actuator orientation with respect to the balance axis system allowed for determination of the applied balance loading.

A total of 57 calibration loading sequences were performed for a total of 1240 calibration points. Table 1 presents the static calibration test envelope. Repeat runs were performed to assess the repeatability of the calibration test setup and data trends. Balance data was acquired during the loading and unloading phase of each load sequence. The use of hydraulic actuators did not provide the required control to duplicate the exact loading during the load and unload phase. However, the same number of points at approximately the same loading were acquired while loading or unloading the balance. Loads up to 22,000 lb for NF and 4,400 lb for AF and SF were applied at the balance moment center. Balance pitch and roll moments were introduced by applying a normal force at a radial location of 3.583 ft from the center in the longitudinal and lateral plane, respectively. Balance pitch and roll moments were also introduced by applying axial and side forces at a height of 5.36 ft above the balance moment center. The maximum balance pitch and roll moment loading was 35,800 ft-lb.

The static calibration data were analyzed to determine a coefficient matrix which includes gage interactions. The method of least squares was used to curve fit the calibration data and to determine the calibration coefficients. Curve fit calculations were performed for the AF and SF voltages and for the digitally resolved voltages for NF, PM, and RM.

The resulting S/DRB static calibration coefficient matrix includes first and second order interaction correction terms for single balance gage loading and first order interaction correction terms for combined balance gage loading (two loads applied simultaneously). The balance was assumed to be bi-directional: separate curve fits were performed on the data for a positive and a negative gage loading. The calibration matrix contains separate coefficients for converting positive and negative gage voltages to engineering unit data and for correction due to balance gage interactions. This coefficient matrix is used in the S/DRB data reduction program to convert the balance gage voltages to engineering unit data. This program uses an iterative scheme to correct the balance data for gage interactions. The balance data reduction methodology is similar to the method used for the data reduction of standard six-component strain gage sting balances used in the NASA Ames wind tunnels (Ref. 5). The balance axis system makes a +1.377 deg yaw angle with the RTA longitudinal plane. The balance data reduction program corrects for this angle offset when converting the balance loading from the balance to the hub axis system.

**Results and Discussion**

The static calibration matrix was used in the S/DRB data reduction program to calculate the balance loading from the static calibration voltage data. The error between the predicted balance loading and the known applied calibration loading was calculated. The standard deviation of these errors was less than 0.3 percent of the balance gage capacity for all the balance gages as shown in Table 2 (case 1).

To assess the balance accuracy and the impact of the data reduction/analysis procedures, the static calibration data base was re-analyzed several ways. A 5-by-5 linear calibration matrix was calculated using all the data in the static calibration data base (Table 2, case 2). A second 5x5 linear calibration matrix was calculated using a subset of the data base: only those data points whose loading approximately matched the shake test load envelope were used. A data point was included in this subset if the balance loading was less than: 1,000 lb for NF, 3,750 ft-lb for PM and RM, and 1,000 lb for AF and SF. This subset contained 240 data points versus 1240 data points for the complete static calibration data base. The balance calibration voltage data were converted to engineering unit data using these two linear calibration matrices and the error between the calculated balance loading and the applied balance calibration loading was determined. This calculation was done both for the subset of the static calibration data base (Table 2, case 3) and for the complete data base (Table 2, case 4). The standard deviation of these errors was determined and the results are shown in Table 2.

Comparing case 1 and case 2 results in Table 2 shows that the accuracy of the prediction of the balance calibration loading decreases if non-linear gage interactions terms are deleted. Case 3 of Table 2 shows that the prediction accuracy is excellent for the calibration matrix calculated from the data base subset when applied to the very same database subset. This is to be expected since the data of the subset covers the lower range of the balance load capacity where the balance response tends to be very linear. However, as expected the accuracy of using such a calibration matrix outside of its calibration range results in a much reduced balance accuracy as shown by the large increase of the standard deviation of error for case 4 in Table 2.

## Dynamic Balance Calibration

This section will describe the test setup and test procedures used during the dynamic calibration of the Rotor Test Apparatus Steady/Dynamic Rotor Balance. The test configurations and the test envelope are also discussed as is the type of data acquired.

### Test Setup

The Rotor Test Apparatus was mounted on the three-strut model support system of the 40- by 80-Foot Wind Tunnel. The rotor plane was approximately 22 ft above the tunnel floor. An extensive shake test was performed to obtain the balance/stand frequency response functions which represents the dynamics of the RTA installation. Figure 4 shows the RTA installed in the test section of the 40- by 80-Foot Wind Tunnel during the shake test. The 8 ft model support struts with 3 ft tips are installed onto a T-frame, which in turn is supported by the wind tunnel scale system.

The rotor hub was replaced by special shake test hardware, which allowed for applying loading with and without the rotor shaft rotating. The shake test hardware consisted of a shaft with a radial bearing installed at the appropriate hub height and a thrust bearing at the end of the shaft. These two bearings allow for the application of static or dynamic loads on a rotating shaft: in-plane hub shear load for the radial bearing and thrust load for the thrust bearing. The outer bearing race is prevented from rotating using guy-wires secured to a telescoping man lift (Fig. 4).

A calibration fixture was attached to the thrust bearing fixture which allowed for vertical load application at the shaft center and at a radial moment arm. The moment carrying capability of the thrust bearing under rotation limited the moment arm to 1 ft. Vertical dynamic loading at the 1 ft moment arm represented the out-of-plane hub shear forces (thrust) and dynamic hub moments. The two bearings allowed for the dynamic in-plane shear load application while applying a steady vertical force at the shaft end, i.e. a thrust force.

Two circular platters were secured to the shaft just below and above the radial hub bearing. Semi-circular weights of 61.1 lb (half-donuts) were installed onto each of these two platters to simulate the hub and blade weight. By adding or removing weights the total shake test mass can be varied to represent the mass of different rotor systems. The vertical cg of the shake test hardware is located at the radial bearing center, which represents the hub location.

### Test Procedures

A hydraulic actuator was used to excite the model and the support system at the nominal hub height of 6.1 ft above the balance moment center. One end of the hydraulic actuator was attached to a 5-ft-long extension arm. The other end of the actuator was attached to the hub. The extension arm was attached to an 11,600-lb reaction mass hung from the gantry crane, as shown in Fig. 4. The shaker was aligned with respect to the extension arm, which was in turn aligned parallel to the shake direction. After achieving rough alignment of the actuator and the extension arm using the gantry crane, finer alignment was achieved by applying tension to the guy wires attached between the reaction mass and the tunnel floor. The guy wires also restrained swinging of the reaction mass during actuator excitation. A load cell located between the hydraulic actuator and the hub measured the applied force.

A random excitation from 0-64 Hz at input force levels of up to ±600 lb were applied at the nominal rotor hub height. A 16-channel GenRad 2515 Computer-Aided Test System was used to acquire and store the Frequency Response Functions (FRFs) of the balance forces and moments with respect to the input force load cell. The FRF data were then transfered to a VAX mainframe computer for further data processing.

### Test Envelope

The shake test setup did not allow for the application of pure hub moments. Hub moments were obtained by applying a vertical force at a 1 ft radial moment arm from the hub center. This loading results in a hub force (thrust) and a hub moment. The balance also measures a balance force and a balance moment with respect to the balance moment center. An in-plane hub shear force does not

result in a hub moment, but results in a balance shear force and a balance moment due to the vertical separation of the hub and balance moment center. To determine the dynamic calibration matrix for the five component S/DRB a total of five loading sequences were used. The five load sequences are identified in Table 3, which also identifies the directly loaded balance gages for each loading. Note that the last four load sequences in Table 3 result in simultaneous loading of a balance force and a balance moment. For each balance loading setup the FRFs for the following balance readings were acquired: NF1, NF2, NF3, NF4, AF, and SF from the balance gages and the resolved NF, PM, and RM signals from the Balance Analog Monitoring Box.

During the shake test, data for the basic set of five loading sequences shown in Table 3 were acquired at zero shaft rotation and at zero thrust pre-load. Data were also acquired during longitudinal and lateral shear force shaking while applying a steady thrust force to the hub. In addition, some data were acquired with shaft rotation at nominal rotor operating RPMs of 315 and 425 RPM, again without and with a thrust preload.

**Test Configurations**

Shake testing of the RTA S/DRB configuration was performed prior to two 40- by 80-Foot Wind Tunnel test entries in which the Sikorsky 5-bladed Bearingless Main Rotor (SBMR) (Ref. 6) and the BO-105 4-bladed hingeless main rotor (Ref. 7) were tested. The RTA was not removed from the tunnel support system between these two tunnel entries. The hub shake test hardware, however, was re-configured to represent the hub/blade mass of each of these two rotor systems. The weight difference between the two hub/blade systems is 740 lb. The hub/balance center offset was 6.1 ft. In general, the lower and upper limit of the RTA test capabilities are represented by the BO-105 and SBMR rotor systems, respectively.

## Shake Test Results and Discussion

Frequency Response Function data were acquired during extensive shake testing of the RTA in the 40- by 80-Foot Wind Tunnel. Table 4 shows the test envelope at which these FRFs were obtained for the two shake test configurations, representing the SBMR and BO-105 rotor systems. These FRF data were acquired at a zero deg RTA shaft angle, i.e. at zero model angle of attack. Data were acquired to determine the effects of rotor RPM, thrust preload, and hub mass on the balance response due to the dynamic behavior of the RTA and the wind tunnel support system.

Representative data are presented in this paper to illustrate the effect of these test parameters on the FRFs for the RTA balance.

**Basic Shake Test Results (0 RPM, 0 thrust preload)**

Figure 5 presents representative FRFs of the balance gage outputs due to an axial force loading at the hub. The balance moment center is located 6.1 ft below the hub and a hub axial force therefore results in both a balance axial force and a balance pitch moment loading. The shake test hub mass for this FRF data set represents the mass of the BO-105 hub and blades. The loading, measured by the input force load cell, was converted into the corresponding loading seen by the balance. The FRF magnitude axis dimension is in units of $EU_{output}/EU_{input}$, where EU represents engineering units of the corresponding balance output. Forces are presented in $lb_{output}/lb_{input}$, while the moments are presented in ft-$lb_{output}$/ft-$lb_{input}$.

Figure 5 shows significant changes in the dynamic response of the balance over the entire frequency bandwidth. Since the balance flexure design places the balance natural frequencies above 60 Hz, the changes in the dynamic balance response seen in Fig. 5 can be attributed to the dynamic structural characteristics of both the wind tunnel support system and the RTA itself. At low frequencies (< 1 Hz) the FRF for the axial force gage (Fig. 5a) and the pitch moment gage (Fig. 5e) show a ratio of approximately 1 as these are the directly loaded gages. The other three gages, being side force (Fig. 5b), normal force (Fig. 5c), and roll moment (Fig. 5d) show a ratio of approximately 0 at low frequency (< 1 Hz) and indicate the amount of load interaction seen by these gages. The balance gage response/interaction is changed significantly by the balance dynamic response as seen in Fig. 5, indicating the necessity of making dynamic corrections to both the gage sensitivity and gage interaction terms in the balance calibration matrix.

**In-Plane Versus Out-of-Plane Loading**

Figure 5 showed the FRF data for the pitch moment gage due to a horizontal or inplane vibratory load at the hub. During another portion of the shake test, a balance pitch moment was also generated by an out-of-plane force: a vertical vibratory load input was applied 1 ft forward of the rotor shaft in the longitudinal plane of the RTA. In this case, the balance normal force and pitch moment gages are loaded simultaneously.

The pitch moment FRF data obtained by inplane and out-of-plane hub force applications are compared in

Fig. 6. In both cases, the measured pitch moment FRF data are the sum of the response of the PM gage due to a pure pitch moment loading and the interaction response to a force application. Assuming that these force interaction contributions are small, the comparison of the two curves in Fig. 6 shows markedly different balance pitch moment response to pitch moment loading due to inplane versus out-of-plane force loading. The difference could be the result of the difference in the magnitude of PM loading, being 500 ft-lb due to the out-of-plane force loading and 3660 ft-lb due to the in-plane force loading. A second explanation is that the RTA/balance response is considerably different for out-of-plane versus in-plane loading.

**Effect of Shaft Rotation**

Figure 7 shows representative FRFs for the axial and normal force gages under vibratory hub axial force loading without and with shaft rotation of 315 and 425 RPM. The shake test configuration again represents the BO-105 hub and blade mass.

Figure 7a shows that the effect of rotation is minimal at low frequencies for the directly loaded gages (AF in this case). Differences are noted at the higher frequencies (>30 Hz) for both the magnitude and phase data with the 425 RPM showing the greatest differences.

The FRF for the normal force interaction (see Fig. 7b) shows some effect of shaft rotation on magnitude at frequencies greater than 30 Hz, but phase shifts are noticed at frequencies as low as 12 Hz. The FRF data of Fig. 7 for both AF and NF show a resonance at approximately 19 Hz, which is also observed in Figs. 5 and 6. Review of the FRF data plots showed that rotation influences the magnitude of this resonance for all balance gages.

The noted effects of rotation on the FRF data as described above are typical for all balance gage responses under the various applied balance loading: rotational effects are mostly seen in the higher frequency range (above 20-30 Hz) and manifest themselves most clearly as a phase shift.

**Effect of Thrust Preload**

The effect of rotor thrust preload is shown in Fig. 8 with no shaft rotation and in Fig. 9 with a shaft rotation of 315 RPM. The thrust preload was +4,000 lb and the response of the axial force and normal force gages is again shown for a hub axial force vibratory loading. The shake test mass represents the BO-105 rotor system (hub and blade mass).

For the directly loaded balance axial force gage, the effect of thrust load is mainly manifesting itself at frequencies above 30 Hz as seen in Figs. 8a and 9a. These figures also show that the thrust preload has a much greater effect on the magnitude of the resonance at 19 Hz when the shaft is rotating.

Figures 8b and 9b show the interaction response of the normal force gage due to the hub axial force loading. Some magnitude differences are noted at frequencies as low as 5-6 Hz. Again shaft rotation results in a greater magnitude reduction at the resonance frequency of 19 Hz as a result of balance thrust preload.

**Effect of Hub Mass**

The effect of hub mass on the balance frequency response is shown in Fig. 10, again for a vibratory hub axial force loading. The data shown are for zero shaft rotation and zero thrust preload. The directly loaded axial force gage response is shown in Fig. 10a. The dynamic response of the rotor balance above 15 Hz is significantly influenced by the hub mass as shown in Fig. 10a.

The interaction response of the normal force gage to the hub axial loading is shown in Fig. 10b. Differences in the FRF magnitude and phase are seen for frequencies above 10 Hz, while some frequency shifting of the resonance peaks at 7 and 8.3 Hz is also noticed.

The FRF changes due to the hub mass change are typical. Magnitude and phase angle changes due to hub mass are seen as low as 2-3 Hz, mostly for non-directly loaded gages, indicating that the effect of hub mass on dynamic gage interactions is important.

Comparison of Figs. 7 through 10 shows that the effect of hub mass on the balance gages FRFs is much greater than the effects of either shaft rotation or thrust preload.

**Shake Test Data Analysis**

The balance Frequency Response Function data are post-processed to calculate the balance dynamic calibration matrix. This matrix is calculated at each spectral line of the FRF data from the shake test. Random input force excitation from 0 to 64 Hz was applied to the rotor hub. The GenRad Computer-Aided Test System acquired and stored the FRFs of the balance forces and moments with respect to the input force load cell. A 512-

point Fast Fourier Transform (FFT) was performed to obtain the FRF data. The spectral line resolution is 0.125 Hz.

In analyzing the FRF data at each spectral line it is assumed that the vibratory loading is similar to a three point quasi-steady load application, being negative L, zero, and positive L, where L is the magnitude of the vibratory loading. Lacking further information the assumption is made that the gage response is linear over the load range and that the gage response at zero loading is indeed zero (no-hysteresis). The FRF data obtained at each spectral line during the shake test therefore represents the curve fit slope of the interaction term due to the applied single or combined loading.

A minimum of five unique balance load cases are required for the five component rotor balance to determine a 5-by-5 dynamic calibration matrix. These five loading sequences were identified in Table 3 and provided a total of 25 FRF curves. Note that a single balance load application occurred only for the thrust loading. The remaining four load sequences resulted in a simultaneous loading of a balance force and a balance moment (see Table 3).

The shake test data analysis program brings the FRF magnitude and phase data into complex format. The program then calculates the 5-by-5 dynamic response matrix at each spectral line. Each element in this response matrix represents the FRF value of a balance gage due to a single balance gage loading. The complex response matrix is subsequently inverted to obtain the complex dynamic calibration matrix at each spectral line.

### Wind Tunnel Balance Data Processing

The balance calibration coefficients in the static calibration matrix represent the response of the various balance gages to a single balance gage loading (i.e. only one balance gage is assumed to be directly loaded) and double gage loading (two balance gages loaded simultaneously). The static (steady) data from the balance is processed using an iterative scheme to account for the fact that during an actual wind tunnel test simultaneous loading of all five balance gages occurs and that a balance gage response is the result of a direct gage loading and of gage interactions due to loading on the other balance gages.

The dynamic data from the balance is processed in much the same manner as the static or steady data from an gage interaction sense, except that only first order single load interaction corrections are applied. The dynamic calibration matrix is the inverse of the balance dynamic response matrix and therefore inherently accounts for the multiple balance gage loading during the tunnel test. The matrix inversion fulfills the same role as the iterative scheme used in the static balance data reduction. The assumption of balance bi-directionality and the inclusion of non-linear interaction terms prevents the inversion of the complete static calibration matrix.

The first step in the wind tunnel data processing is the acquisition of eight revolutions of data synchronized to the once-per-revolution of the rotor. The typical sampling rate used in the NFAC facility is 64 samples/revolution. The Rotor Data Reduction System (RDRS) program is used for the off-line data reduction. The balance data are harmonically analyzed into the frequency domain and corrected for the analog filter settings and time skew. The balance data are then corrected at each harmonic for both magnitude and phase using the dynamic calibration matrix.

The shake test FRFs are composed of a finite number of spectral lines with a spectral density of 0.125 Hz. The RDRS program determines the FRF spectral lines (frequencies) nearest to each wind tunnel test harmonic, n/rev, and performs a linear interpolation on the elements of the balance dynamic calibration matrix at the next higher and lower spectral line to determine the dynamic calibration matrix at the n/rev harmonic frequency. If the n/rev harmonic frequency exceeds the range of the shake test FRF data (>64 Hz, approximately 9-12 per rev for a full-scale helicopter rotor) the static, linear 5x5 calibration matrix is used instead.

### Hub Imbalance Runs

Data from two hub imbalance tests were acquired and were used to evaluate the accuracy of the dynamic calibration matrix/methodology for the prediction of 1/rev balance loading for frequencies from 2 to 7 Hz.

#### SBMR hub imbalance configuration

The baseline SBMR balance shake test configuration was operated from 140 to 375 RPM, corresponding to a 1/rev frequency from 2.3 to 6.25 Hz. This spinup was performed with all half-donut weights installed (balanced hub). One 61.1 lb half-donut weight was subsequently removed from the upper weight stack. The remaining half-donut causes a hub mass imbalance of 61.1 lb with the mass cg being at the 0.46 ft radial location. The vertical height of this hub imbalance cg was at 6.6 ft above the balance moment center. This imbalanced hub

configuration was spun up from 140 to 330 RPM, corresponding to a 1/rev frequency from 2.3 to 5.5 Hz.

**BO-105 hub imbalance configuration**

A hub imbalance run was also performed with the actual BO-105 rotor hardware. A mass imbalance in the BO-105 rotating system was generated by the addition of a 14.6 lb weight at one of the blade attachment points. The radial location of the mass cg was at approximately 1.20 ft. The imbalance mass cg was at a vertical height of 6.02 ft above the balance moment center. The rotor blades were not installed during this run. Thus the "rotor system mass" during this hub imbalance run was approximately 250 lb lighter than the hub mass used during the BO-105 shake test. Prior to this hub imbalance run, the rotor hub itself was dynamically balanced to within ±20 lb at the design rotor RPM of 425 RPM. Balance data for both the balanced and imbalanced hub were acquired for rotor shaft RPMs varying from 120 to 425 RPM (from 2 to 7 Hz).

**Hub Imbalance Test Results**

Figures 11 through 19 show the load prediction results for the hub imbalance runs for the SBMR and BO-105 shake test configurations. These predictions are compared to the expected balance loading due to the known hub imbalance and the resulting hub forces due to the centrifugal loading. Only a 1/rev loading is expected due to the hub imbalance; the expected loading at the n/rev harmonics, n>1, are zero. The effects of hub mass, shaft rotation, and thrust preload on the hub imbalance load predictions will be discussed.

**Effect of Hub Mass**

Figures 11 through 14 show the load predictions for the SBMR and BO-105 hub imbalance tests using the static calibration matrix and two dynamic calibration matrices. Separate dynamic calibration matrices were calculated from the shake test data (FRFs) for the SBMR hub mass and the BO-105 hub mass configurations. These matrices are referred to as the SBMR dynamic calibration matrix and the BO-105 dynamic calibration matrix, respectively. These dynamic calibration matrices are derived from the shake test FRF data for the non-rotating shaft at zero thrust preload. The two shake test configurations differ only in the amount of rigid, concentrated mass attached to the hub. The BO-105 rotor system weight (hub and blades) is approximately the same as the SBMR hub-only weight. The present data set therefore provides a unique opportunity to evaluate the balance accuracy in predicting a known hub imbalance loading when using a dynamic calibration matrix determined from a shake test with and without simulated blade mass. This is the case for the SBMR and BO-105 dynamic calibration matrices, respectively, for the SBMR hub imbalance runs.

Figure 11 shows the comparison of the expected versus the calculated balance 1/rev loading for the SBMR hub imbalance test from 2.4 to 5.5 Hz. The shaft RPM was restricted to 330 RPM (5.5 Hz) for this hub imbalance test due to excessive shaking of the RTA model. The calculated loading using the static calibration matrix show considerable errors. Figure 11 also shows the load predictions using the dynamic calibration matrices. Using either the SBMR or BO-105 dynamic calibration matrix improves the predictions across the measured frequency range from 2.4 to 5.5 Hz as compared to the prediction results of the static calibration matrix. The dynamic calibration matrix obtained from the SBMR shake test provides more accurate load predictions as compared to the results using the dynamic calibration matrix obtained from the BO-105 shake test.

Figure 12 shows the balance load predictions at the n/rev harmonics, for n>1. The expected n/rev loading is zero. The n/rev harmonic predictions using the dynamic calibration matrices only go up to 64 Hz since this is maximum frequency at which FRF data was obtained. The predictions from the static calibration matrix go up to 100 Hz, being the filter setting for the low pass analog filter. Figure 12 also shows that in general the static calibration matrix results in lower n/rev loading than the predictions using the dynamic calibration matrices. This is especially true for the frequencies above 20 Hz. The dynamic calibration matrix based upon FRF data for the BO-105 hub mass tends to show slightly lower loading as compared to the predictions using the SBMR dynamic calibration matrix.

The results of the hub imbalance test run for the BO-105 rotor configuration are presented in Figs. 13 and 14. The expected 1/rev hub imbalance loading with respect to the balance moment center is shown in Fig. 13 and is compared to the predicted loading using the static and the dynamic calibration matrix approach. Reducing the data with the static calibration matrix results in fairly large scatter in the prediction accuracy, especially the force prediction (Figs. 13a-c). The use of a dynamic calibration matrix improves the load prediction accuracy. Figure 13 shows smaller prediction error when using the BO-105 dynamic calibration matrix versus the SBMR dynamic calibration matrix. Large errors remain at the 7 Hz location, especially for the normal force gage, which

measures rotor thrust. The 7 Hz frequency corresponds to a structural support resonance frequency.

Figure 14 shows the calculated balance loading at the n/rev harmonics, where n>1 and for frequencies up to 100 Hz. The expected loading at the n/rev harmonic is zero and the data points in Fig. 14 therefore represent the prediction error. Figure 14 shows that the static calibration matrix provides reasonably small prediction errors over most of the frequency range with some larger errors around 20 Hz. The SBMR dynamic calibration matrix results in considerably large prediction errors above 20 Hz and especially above 40 Hz. The results using the BO-105 dynamic calibration matrix provide increased errors as compared to the static prediction results, but show much lower errors as compared to the results using the SBMR dynamic matrix.

In terms of percent of the S/DRB dynamic load capabilities, Fig. 14 shows that the prediction results for the n/rev loading, n>1, using the BO-105 dynamic calibration matrix are in general better than 100 lb for axial force (<10 percent of 1,100 lb capacity), 50 lb for side force (<5 percent of 1,100 lb capacity), 100 lb for normal force (2 percent of 5,500 lb capacity), 400 ft-lb of roll moment (<5 percent of 8,920 ft-lb capacity), and 750 ft-lb of pitch moment (<9 percent of 8,920 ft-lb capacity). Table 5 summarizes the balance accuracy for the 1/rev loading for the SBMR and BO-105 hub imbalance tests, when using the dynamic calibration matrix determined from FRFs for the SBMR and BO-105 shake test configurations, respectively.

Figures 15 and 16 show the predictions for the BO-105 hub imbalance test in percent of the applied 1/rev hub imbalance loading. The predictions use the BO-105 dynamic calibration matrix, which was shown in Fig. 13 and 14 to provide the better dynamic prediction results as compared to using the SBMR dynamic calibration matrix. Figure 15a shows that the prediction of the 1/rev shear forces is better then 10 percent of the applied hub imbalance loading. Notice again the large error in the prediction of the normal force, NF, which occurs at the structural support mode around 7 Hz. Figure 15b shows that in general the prediction of the 1/rev balance moment is also better than 10 percent of the applied moment.

Figure 16 shows the n/rev harmonic data , for n>1, as a percent of the applied 1/rev loading. Expanded scales are used for the vertical axis in Fig. 16. Some of the data showing extremely large prediction errors in Fig. 14 are eliminated in Fig. 16. Figure 16a shows that the side force prediction error is in general less than 5 percent of the applied 1/rev loading. Both the axial and normal force loading shows larger errors, but in general the errors are less than 10 percent of the applied 1/rev loading. Figure 16b shows the moment data in percent of the applied 1/rev balance moment and shows that the roll moment error is generally smaller than the pitch moment error, but that the prediction error for both moments is generally less than 8 percent of the applied 1/rev balance moment. Note that the static calibration also showed larger errors for the axial force and pitch moment predictions as compared to the side force and roll moment predictions (see Table 2, cases 2-4).

The results of Figs. 11 through 16 show that the hub imbalance loading is most accurately predicted when using the dynamic calibration matrix obtained from the Frequency Response Function data for the shake test hub configuration which most closely matched the actual mass of the imbalanced hub configuration.

**Effect of Shaft Rotation**

Figure 17 presents the prediction of the 1/rev hub imbalance loading for the BO-105 hub imbalance test based upon the BO-105 dynamic calibration matrices obtained from the FRF data without shaft rotation and with shaft rotation of 315 and 425 RPM. The dynamic calibration matrices based upon the 0 RPM and 315 RPM FRF data result in 1/rev load prediction errors of essentially similar magnitude. The "0 RPM" matrix provides slightly better predictions for axial force and pitch moment as compared to the "315 RPM" matrix. However, using the dynamic calibration matrix obtained from the 425 RPM FRF data results in large prediction errors. It should be noted again that the FRF data shows a structural support mode at approximately 7 Hz which corresponds to a rotor shaft rotation rate of 425 RPM. These data are therefore suspect and should not be used in the determination of a dynamic calibration matrix.

The 1/rev load predictions for the SBMR hub imbalance test using the dynamic calibration matrix based upon the FRF data obtained at 0 and 315 RPM shaft rotation also provided similar results. Again the "0 RPM" matrix gave slightly better predictions for axial force and pitch moment as compared to the "315 RPM" matrix.

The data indicate that no real improvement in the 1/rev load prediction is obtained by using FRF data from a shake test with the shaft rotating. This was not unexpected since the effect of the shaft rotation on the FRF data was small for the lower frequency range as discussed previously and illustrated in Fig. 7. Differences in the FRF magnitude and phase at higher frequencies due to shaft rotation were observed (Fig. 7) and some larger

effects on the higher harmonic loading were therefore expected. Some improvements, most notably in the force prediction, were indeed observed for the BO-105 predictions of the n/rev harmonic loading, n>1, when using the dynamic calibration matrix for the 315 RPM FRF data (Fig. 18) as compared to the "0 RPM" matrix (Fig. 16). To a somewhat lesser extent, such improvements were also observed for the SBMR hub imbalance test.

**Effect of Thrust Preload**

The expected normal force loading for the hub imbalance tests is zero. Therefore, using a dynamic calibration matrix based upon FRF data obtained with a thrust preload present would be inappropriate. However, for completeness such a dynamic calibration matrix was also used to predict the hub imbalance loading. The results showed increased errors in the 1/rev hub force and moment loading and such errors increased further if the FRF data for the shake test with thrust preload and shaft rotation was used for the dynamic matrix determination.

**Dynamic Zero Correction**

Prior to performing the hub imbalance test an RPM sweep was performed for the balanced hub to obtain a base line case for the balance loading. These data were used to determine the effects of a dynamic zero correction. The data from the imbalanced hub run was corrected in magnitude and phase based upon the data from the balanced hub run. These corrections were performed in the complex domain for each of the harmonics up to 64 Hz.

The 1/rev hub imbalance load predictions for the BO-105 hub configuration with the dynamic zero correction applied are shown in Fig. 19. The balance loading is again shown in normalized form by dividing the balance forces by the applied 1/rev imbalance shear load and the moments by the applied 1/rev imbalance moment. Comparison of the data of Fig. 19a with the predictions of Fig. 15a (no dynamic zero correction) shows that a slight improvement in the force prediction is obtained by incorporating the dynamic zero correction. However, such a zero correction results in a consistent under prediction of the balance moments in Fig. 19b.

Figure 20 shows the load prediction errors for the n/rev harmonics, for n>1, with the dynamic zero correction applied and again normalized by the applied 1/rev imbalance force and moment at the balance moment center. Comparison of the dynamic zero corrected data of Fig. 20 with the data of Fig. 16 (no dynamic zero correction applied) shows no consistent reduction in the load prediction error due to the zero correction. Plotting the n/rev normalized data for the balanced hub run resulted in a scatter plot similar to that of Fig. 16 (no zero correction) and of Fig. 19 (with zero correction). Further review of the harmonic data revealed that the magnitude of the n/rev harmonic data was often similar for the balanced and imbalanced hub. The relative phasing between the balanced hub and imbalanced hub harmonic data, however, was such that no consistent reduction in the n/rev load prediction error could be obtained by applying a dynamic zero correction.

**Effect of Model Angle of Attack**

The BO-105 imbalanced hub test included an angle of attack sweep from -15 to +10 deg at a rotor rotation rate of 425 RPM, which is equivalent to 7 Hz. The normalized 1/rev load prediction as a function of model angle of attack is shown in Fig. 21. The expected normalized 1/rev loading for the axial and side forces and for the roll and pitch moments is 100 percent, if independent of the angle of attack. The expected normal force is zero, although the data in Fig. 15 had revealed a normalized normal force error of 65 percent at 7 Hz.

The data in Fig. 21 shows a clear dependency of the load prediction error on the model angle of attack for all balance gages. Side force and roll moment show the least effect of model angle of attack as would be expected since these loadings are in the lateral plane of the RTA model. The effect of angle of attack on the loading for the balanced hub was shown to be minimal. An angle of attack sweep from 0 to -10 deg for the SBMR hub imbalance configuration also showed a load prediction variation with angle of attack.

It is believed that the frequency response of the RTA and the wind tunnel model support system is dependent upon the model attitude and manifested itself in the prediction errors at angle of attack as observed in Fig. 21. Therefore, the dynamic calibration matrix calculated at zero deg angle of attack should only be used at zero deg angle of attack. The model angle of attack effect on the balance loading is fairly linear (Fig. 21). It may therefore be possible to limit a future shake test to acquiring the balance FRFs at a few model angles of attack over the expected test range. The dynamic calibration matrices at these model angles of attack would be determined from the corresponding FRFs. The dynamic calibration matrix at an intermediate model angle of attack could then be obtained from an interpolation between these dynamic calibration matrices

## Discussion

The dynamic calculations described above used the analog signals for NF, PM, and RM provided by the Balance Analog Monitoring Box (BAMB). In the RDRS program the harmonics for the individual flexure normal force signals (NFi, i=1-4) were also combined to produce the NF, PM, and RM harmonics, which were then corrected for magnitude and phase using the dynamic calibration matrix at each harmonic frequency. Comparison of the 1/rev load predictions obtained from the analog derived signals and those from the digitally derived signals for NF, PM, and RM showed very similar results. The observed small differences are attributed to the small phase shift between the input and output signals of the BAMB. This phase shift is a result of the analog processing being performed within the BAMB and the associated time delay caused by the analog circuitry. This phase shift is not accounted for when digitally determining NF, PM, and RM. Additional (round-off) errors are introduced by combining the harmonics of the individual NFi signal into the harmonics for NF, PM, and RM, versus obtaining these harmonics from the FFT of the analog derived signals for NF, PM, and RM.

The accuracy of the dynamic load prediction capabilities of the balance were evaluated using data from an RPM sweep for an imbalanced hub. The moments seen by the balance in this case are solely due to hub inplane shear forces. The balance moment loading during actual wind tunnel testing is caused by both inplane and out-of-plane forces on the rotor blades. As was seen in Fig. 6 the balance Frequency Response Function is quite different due to balance moments caused by inplane versus out-of-plane force loading. Also note from Table 3 that the balance moments during the shake test due to inplane force loading were a factor 7 larger than the moments due to out-of-plane force loading. It would therefore be expected that the elements within the dynamic calibration matrix are "weighted" towards inplane load predictions. No verification data existed to evaluate the accuracy of predicting the out-of-plane force and resulting roll and pitch moments.

The imbalanced hub test also provided for only 1/rev loading from 2 to 7 Hz. The accuracy of the balance at higher frequencies was evaluated by determining how well the zero loading at the n/rev harmonics, n>1, was predicted. A more valuable evaluation would have been to determine how well the balance could measure actual non-zero loading at these higher frequencies. However, such data are not available.

The static balance calibration showed a nonlinear response for the various balance gages under loading. Dropping the non-linear terms in the calibration matrix results in decreased balance accuracy as shown in Table 2 (case 1 versus case 2). The shake test provided a vibratory load around a zero-mean loading for the various balance gages. The resulting Frequency Response Functions for the balance gages can be interpreted as the local slope (tangent) to the gage load versus gage response curve at zero mean loading. The balance loading during actual wind tunnel testing will result in vibratory loads around a non-zero mean loading for the various balance gages. Because of the noted balance gage non-linearities it can therefore be expected that the tangent to the balance load-gage response curve will change with the balance gage preload. As a result, the balance accuracy in predicting vibratory loads is expected to decrease at non-zero balance mean loading when using the dynamic calibration matrix obtained from the balance shake test at zero mean loading. However, no data exist against which to evaluate and quantify this expected decrease in balance accuracy. The imbalanced hub tests provided a 1/rev vibratory load around a zero mean loading.

An error analysis of the measured, dynamically corrected balance loading was performed to determine how much additional hub imbalance was required to explain the difference between the expected and measured 1/rev loading. This additional hub imbalance could be caused by an slight imbalance of the "balanced" hub or due to an imbalance loading caused by shaft deflection under loading. Both scenarios were analyzed and it was found that a minor hub imbalance (balanced hub mass located at a radial location/offset of 0.12 in) would cause the noted discrepancies in the shear force and moment loading. Data from accelerometers attached to the non-rotating outer race of the radial bearing in the SBMR shake test setup revealed hub displacements of this order during the SBMR imbalanced hub test.

## Recommendations for Future Work

The wind tunnel data reduction program transforms the measured balance loading to the hub to provide a measurement of the hub loads for the rotor system being tested on the RTA. However, the balance measures the total rotor loads from the dual load path formed by the rotor shaft and the rotor control system (pitch link loads). Means to correct the balance data for the control system loads so as to obtain corrected hub loads should be investigated. This requires acquisition of balance FRF data while applying vibratory loading through the control system loadpath. Limited FRF data were acquired during the BO-105 shake test by applying vibratory loading

(<100 lb) to the non-rotating pushrods of the RTA control system. These data are presently being analyzed. However, no data exist against which to evaluate and quantify the control system dynamic hub load correction.

Future shake tests should acquire accelerometer data at the hub in both on-axis and off-axis load directions to aid in determining the hub displacements and the effects of inertial loading on the balance response.

Shake testing of the RTA tunnel installation at various angles of attack should be performed to investigate the effect of model angle of attack on the balance dynamic response (FRFs). These data can be used to determine if accurate balance load predictions can be obtained by using a dynamic calibration matrix obtained from the interpolation over model angle of attack of the dynamic calibration matrices, determined at only several wind tunnel test angles of attack.

The accuracy of the balance load predictions was evaluated against the expected loading from an imbalanced hub test. This provided only 1/rev balance loading up to 7 Hz. The effects of shaft rotation and especially hub mass on the balance Frequency Response Functions is most noticable at frequencies above 15 Hz. A means to introduce vibratory loading at higher frequencies needs to be developed to properly evaluate and quantify the balance accuracy at higher frequencies. Such loading should include in-plane and out-of-plane forces and hub moments.

## Concluding Remarks

The static and dynamic calibration efforts of the rotor balance of the recently modified NASA Ames Rotor Test Apparatus are described. The five-component balance was shown to be accurate better than 0.5 percent of gage capacity for all balance gages in the prediction of static loads.

Data from an imbalanced hub test with rotor rotational speeds from 2 to 7 Hz were used to evaluate the dynamic calibration method. Results show that a major improvement in the prediction of 1/rev oscillatory rotor loads is possible using a dynamic calibration matrix as compared to using the static calibration matrix. Using frequency response data for the correct hub mass, representing the rotor system (hub and blades), to determine the dynamic calibration matrix, was shown to be essential to obtain accurate dynamic load predictions. The balance predictions of the 1/rev hub imbalance loading was accurate to within 10 percent.

Using frequency response function data from a dynamic calibration test with shaft rotation present to determine the dynamic calibration matrix resulted in minimal improvements in the 1/rev load predictions as compared to the results of the 0 RPM dynamic calibration matrix. The model angle of attack was shown to be major contributor to errors in the 1/rev loading prediction thus restricting the usefulness of the dynamic calibration matrix to zero deg angle of attack. Insufficient data exists to fully evaluate the dynamic calibration matrix approach at the higher harmonics.

## References


1. Lehmann, G.. and Fu, K. -H., "Theoretical And Experimental Investigations On A Six-Component Rotor Balance," Eleventh European Rotorcraft Forum, The City University, London, EC1V OHB, England, September 1983.

2. Gabel, R., Sheffler, M., Tarzanin, F., and Hodder, D., "Wind Tunnel Modeling of Vibratory Loads," 38th Annual Forum of the American Helicopter Society, Anaheim, CA, May 1982.

3. Young, D., and Tarzanin, F., "Structural Optimization And Mach Scale Test Validation of A Low Vibration Rotor," 47th Annual Forum of the American Helicopter Society, Phoenix, AZ, May 1991.

4. Staley, J.A., Matthew, M.B., and Tarzanin, F., "Wind Tunnel Modeling of High Order Rotor Vibration", 49th Annual Forum of the American Helicopter Society, St. Louis, MO, May, 1993.

5. van Aken, J. M., "Description of the Standard Wind Tunnel Balance Program," KU-CRINC Report 7440-3, University of Kansas Center for Research, Inc. April 1988.

6. Norman, T. R., Cooper, C.R., Fredrickson, C. A., and Herter, J.R., "Full-Scale Wind Tunnel Evaluation of the Sikorsky Five-Bladed Bearingless Main Rotor," 49th Annual Forum of the American Helicopter Society, St. Louis, MO, May, 1993.

7. Peterson, R.L., Maier, T., Langer, H.J., and Tranapp, N., "Correlation of Wind Tunnel and Flight Test Results of a Full-Scale Hingeless Rotor," American Helicopter Society Aeromechanics Specialists Conference, San Francisco, CA, January 19-21, 1994.

Table 1. Static balance calibration loading envelope (entries in parenthesis identify negative loading).

| NF lb | PM ft-lb | RM ft-lb | AF lb | SF lb |
|---|---|---|---|---|
| 0-22k | | | | |
| 0-10k | 0-36k | | | |
| 10-20k | 0-36k | | | |
| 0-10k | 0-(36k) | | | |
| 10-20k | 0-(36k) | | | |
| 0-10k | | 0-36k | | |
| 10-20k | | 0-36k | | |
| 0-10k | | 0-(36k) | | |
| 10-20k | | 0-(36k) | | |
| | | | 0-4.4k | |
| | | | 0-(4.4k) | |
| | | | | 0-4.4k |
| | | | | 0-(4.4k) |
| 3.5k-13.5k | 0-36k | 12.5k | | |
| 3.5k-13.5k | 0-36k | (12.5k) | | |
| 3.5k-13.5k | 0-(36k) | 12.5k | | |
| 3.5k-13.5k | 0-(36k) | (12.5k) | | |
| 3.5k-13.5k | 12.5k | 0-36k | | |
| 3.5k-13.5k | (12.5k) | 0-36k | | |
| 3.5k-13.5k | 12.5k | 0-(36k) | | |
| 3.5k-13.5k | (12.5k) | 0-(36k) | | |
| | 0-23.6k | | 0-4.4k | |
| | 0-(23.6k) | | 0-(4.4k) | |
| | | 0-23.6k | | 0-4.4k |
| | | 0-(23.6k) | | 0-(4.4k) |

Table 3. Identification of the directly loaded balance gages for the various shake test loading sequences.

| | NF lb | PM ft-lb | RM ft-lb | AF lb | SF lb |
|---|---|---|---|---|---|
| Vertical loading at shaft center | 600 | | | | |
| Vertical loading at 1 ft forward of shaft center | 500 | 500 | | | |
| Vertical loading at 1 ft to the left of shaft center | 500 | | 500 | | |
| Horizontal loading in longitudinal direction | | 3,660 | | 600 | |
| Horizontal loading in lateral direction | | | 3,660 | | 600 |

Table 2. Accuracy of the static balance calibration load predictions.

| | static calibration matrix format | data base used in error calculation | Standard deviation of error in percent of maximum gage loading NF | PM | RM | AF | SF |
|---|---|---|---|---|---|---|---|
| 1 | non-linear, bi-directional | complete | 0.11 | 0.12 | 0.08 | 0.16 | 0.27 |
| 2 | linear, complete data base | complete | 0.10 | 0.14 | 0.12 | 0.35 | 0.32 |
| 3 | linear, reduced data base | reduced | 0.04 | 0.06 | 0.03 | 0.13 | 0.06 |
| 4 | linear, reduced data base | complete | 0.25 | 0.39 | 0.20 | 0.68 | 0.45 |
| | maximum or 100 % gage loading units | | 22k lb | 36k ft-lb | 36k ft-lb | 4.4k lb | 4.4k lb |

Table 4: Loading envelope for the SBMR and BO-105 shake tests.

a. SBMR data set

| RPM | 0 | 315 | - | 0 | 315 |
|---|---|---|---|---|---|
| Thrust (lb) | 0 | 0 | - | 2000 | 2000 |
| Vertical loading at shaft center | X | X | | | |
| Vertical loading at 1 ft forward of shaft center (long. plane) | X | X | | | |
| Vertical loading at 1 ft to the left of shaft center (lateral plane) | X | X | | | |
| Horizontal loading in longitudinal direction | X | | | X | X |
| Horizontal loading in lateral direction | X | X | | X | X |

b. BO-105 data set

| RPM | 0 | 315 | 425 | 0 | 315 |
|---|---|---|---|---|---|
| Thrust (lb) | 0 | 0 | 0 | 4000 | 4000 |
| Vertical loading at shaft center | X | X | X | | |
| Vertical loading at 1 ft forward of shaft center (long. plane) | X | X | X | | |
| Vertical loading at 1 ft to the left of shaft center (lateral plane) | X | X | X | | |
| Horizontal loading in longitudinal direction | X | X | X | X | X |
| Horizontal loading in lateral direction | X | | | X | |

Table 5. Accuracy of the dynamic balance load prediction for the imbalanced hub tests (1/rev loading, zero deg model angle of attack).

| | NF | PM | RM | AF | SF |
|---|---|---|---|---|---|
| SBMR test (using SBMR dyn. matrix.) | 1.5 | 4 | 8 | 11 | 8 |
| SBMR test (using SBMR dyn. matrix.) | 2 | 5 | 10 | 18 | 12 |
| BO-105 test (using BO-105 dyn. matrix) | 3 | 5 | 4 | 5 | 5 |
| vibratory load capacity | 5500 | 8920 | 8920 | 1100 | 1100 |
| units | lb | ft-lb | ft-lb | lb | lb |

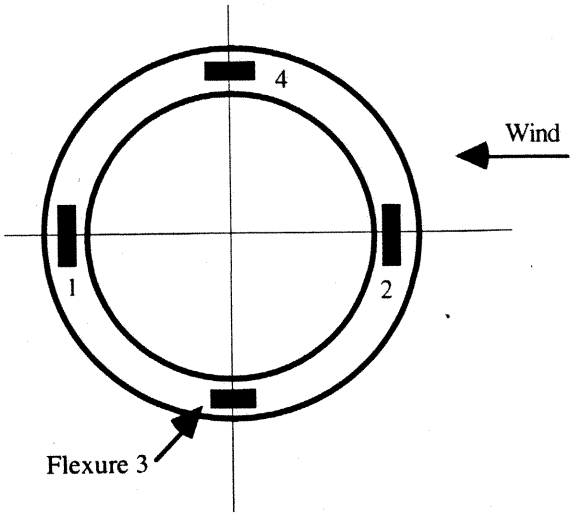


Fig. 1 Schematic top view of the Steady/Dynamic Rotor Balance with flexure identification.

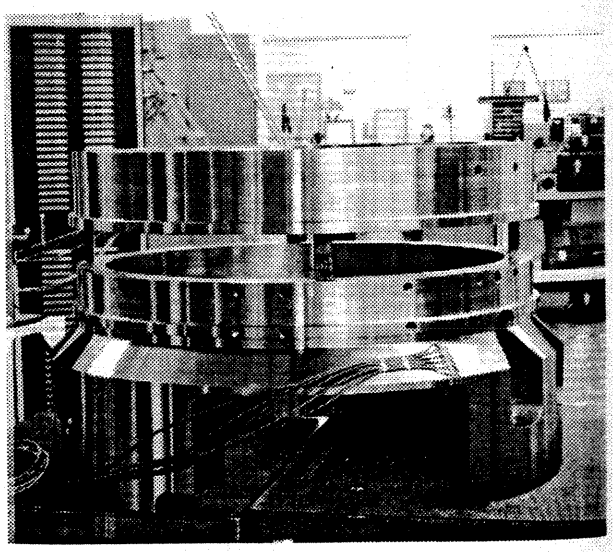

Fig. 2 Steady/Dynamic Rotor Balance.

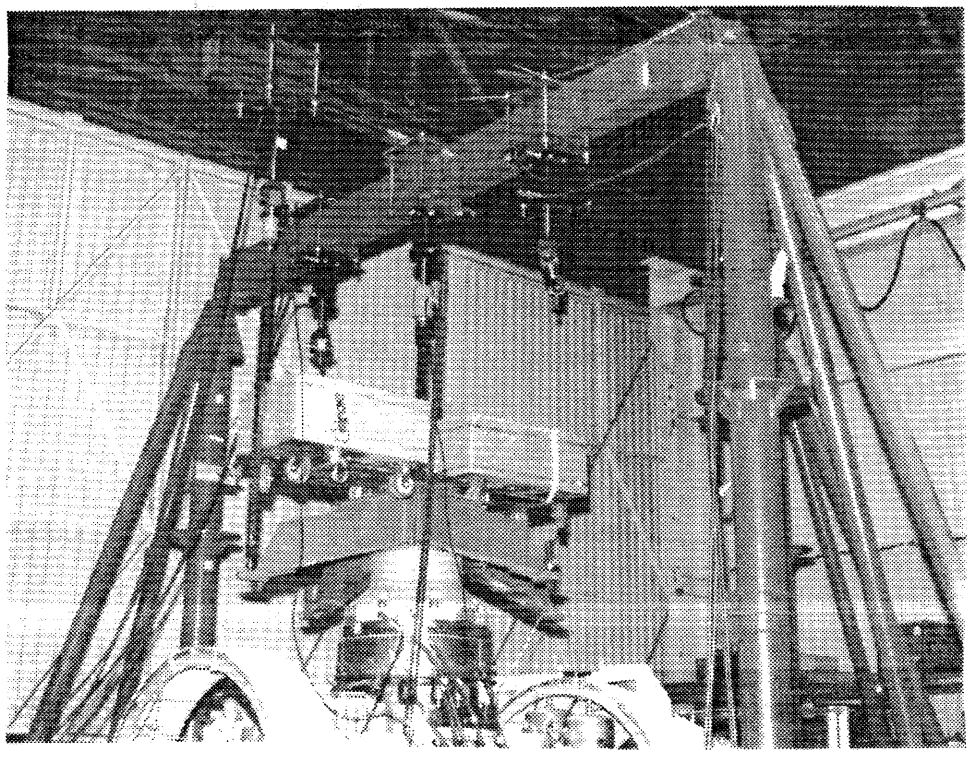

Fig. 3 Test setup for the installed, static balance calibration.

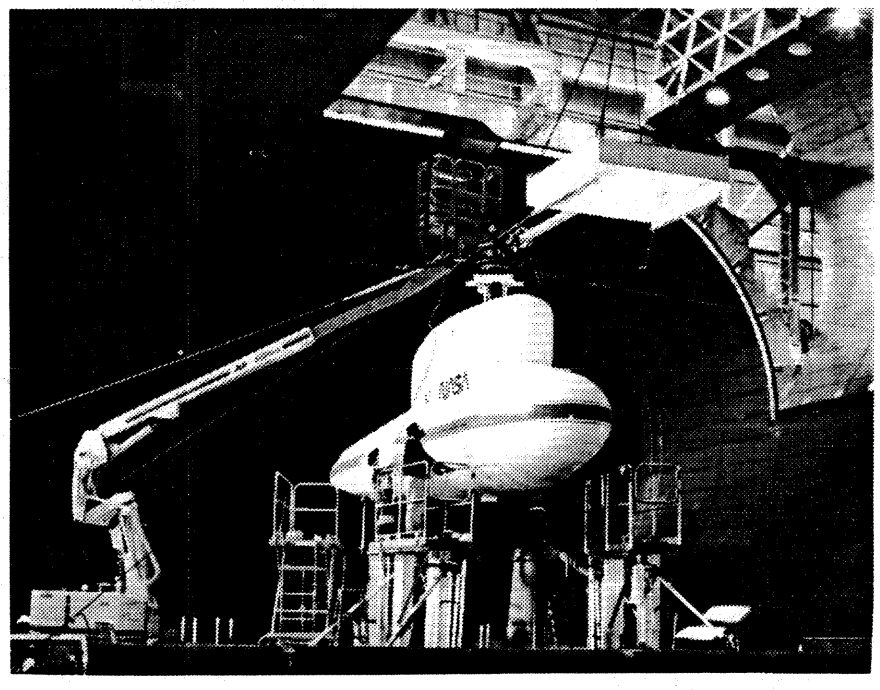

Fig. 4 Test setup for the installed, dynamic balance calibration in the 40- by 80-Foot Wind Tunnel.

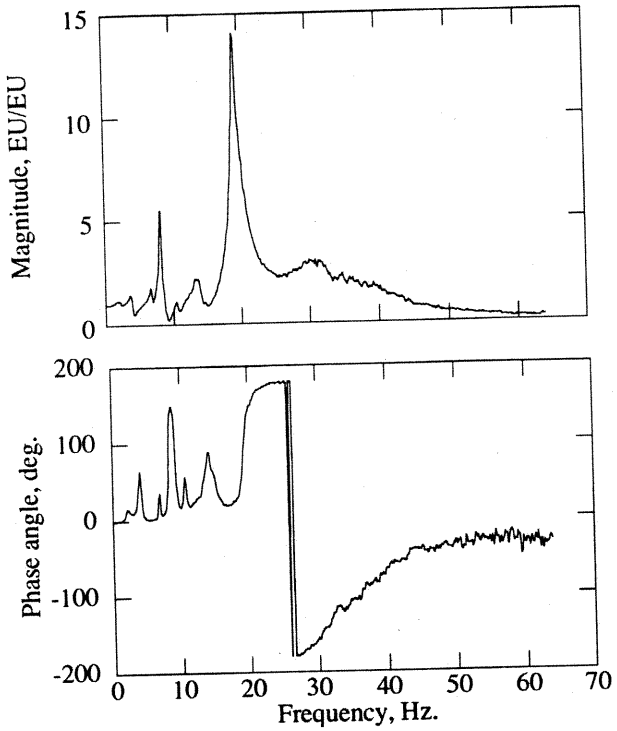


a. Axial force gage response

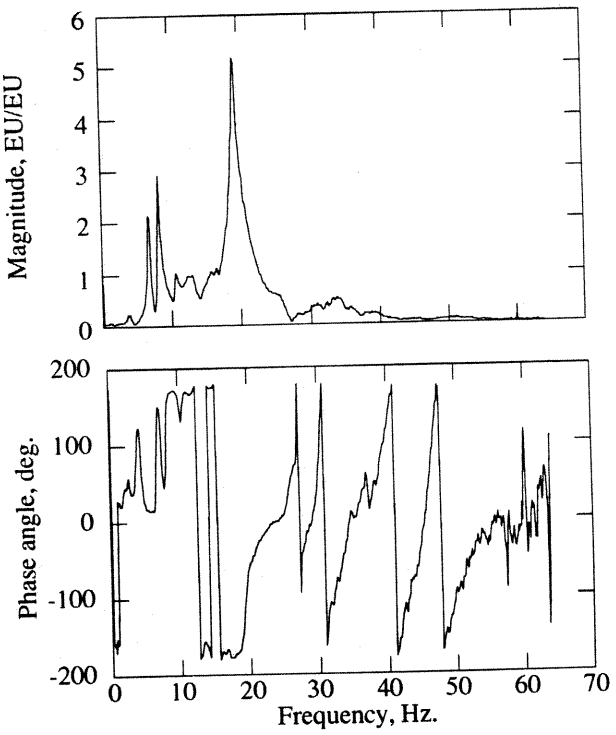


c. Normal force gage response

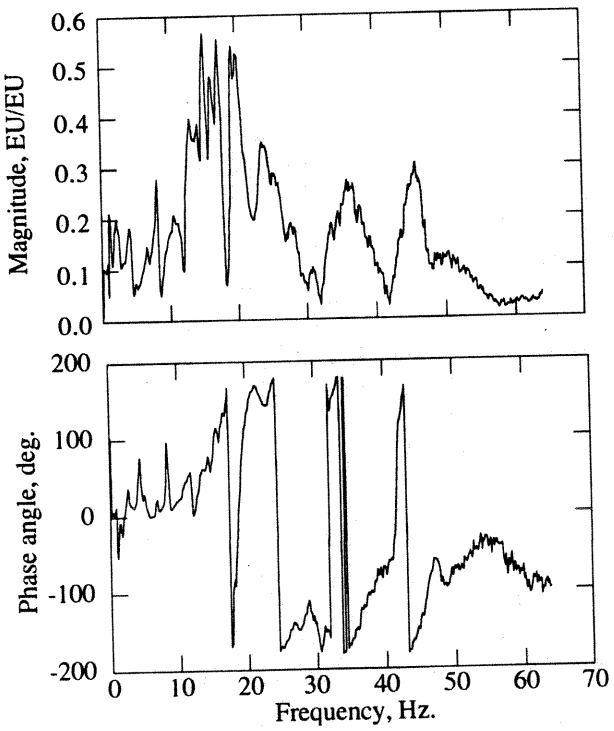


b. Side force gage response

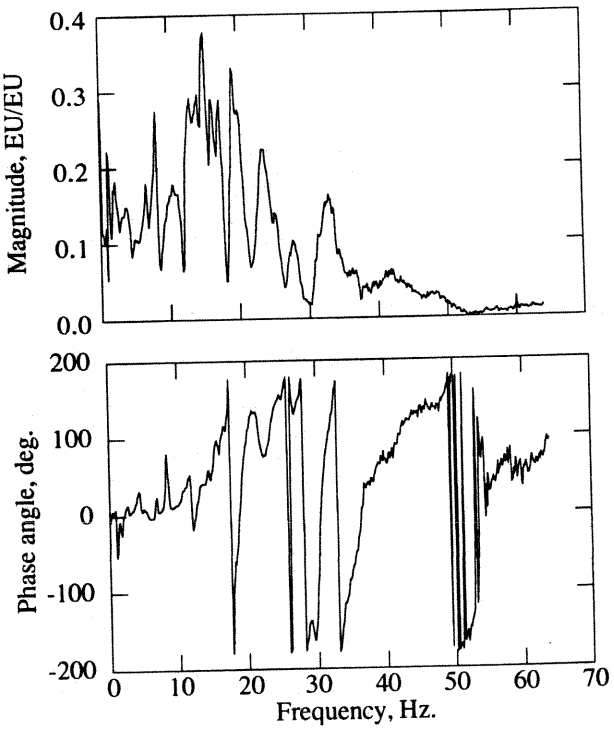


d. Roll moment gage response

Fig. 5 Balance response due to hub axial force loading, simulated BO-105 hub mass.

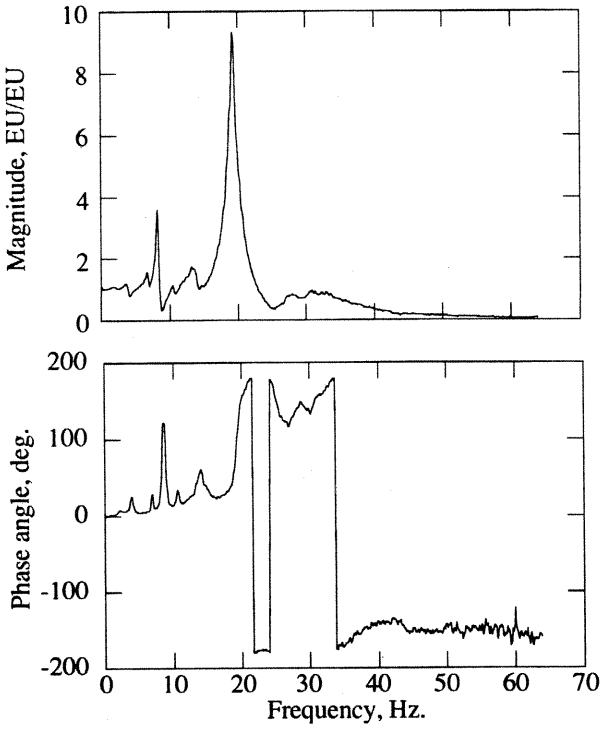


e. Pitch moment gage response

Fig. 5 Balance response due to hub axial force loading, simulated BO-105 hub mass (concluded).

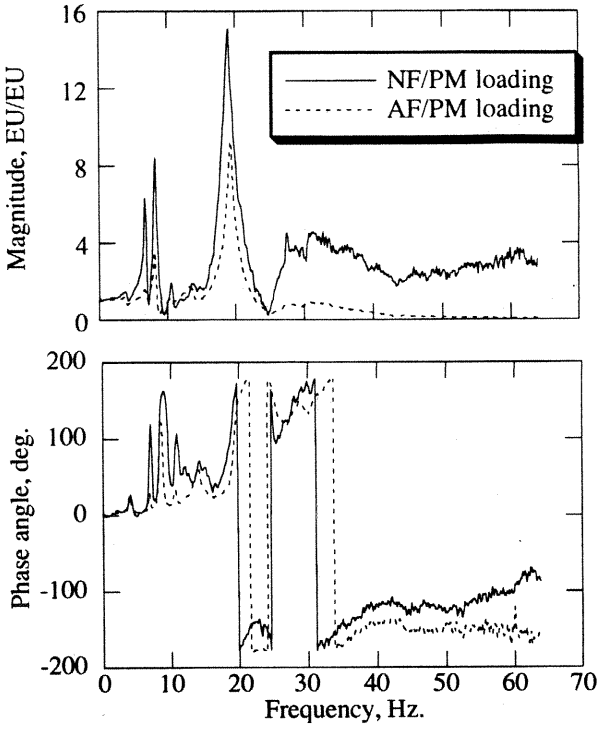


Fig. 6 Balance pitch moment response due to in-plane and out-of-plane hub forces, simulated BO-105 hub mass.

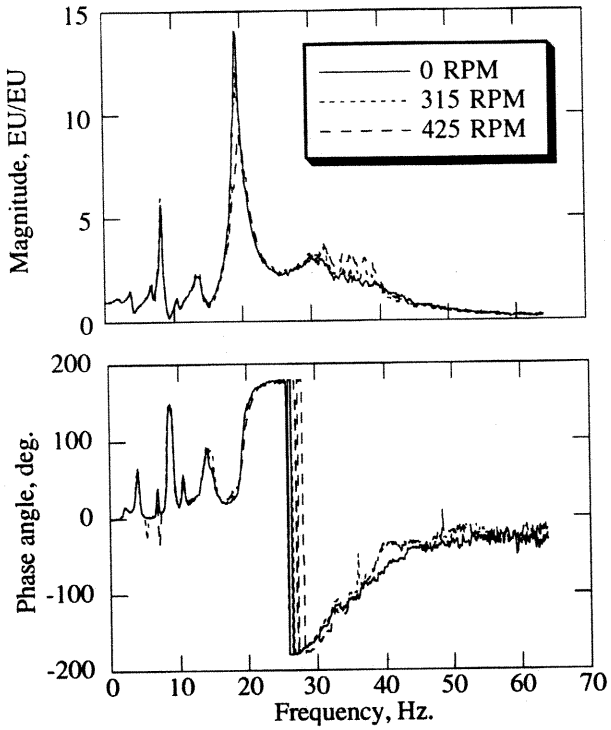


a. Axial force gage response

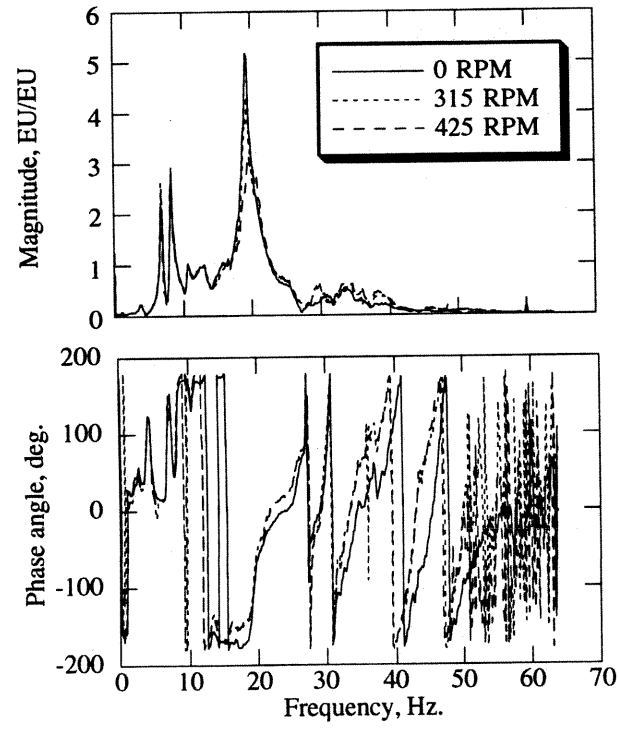


b. Normal force gage response

Fig. 7 Effect of shaft rotation on the balance response under hub axial force loading, simulated BO-105 hub mass.

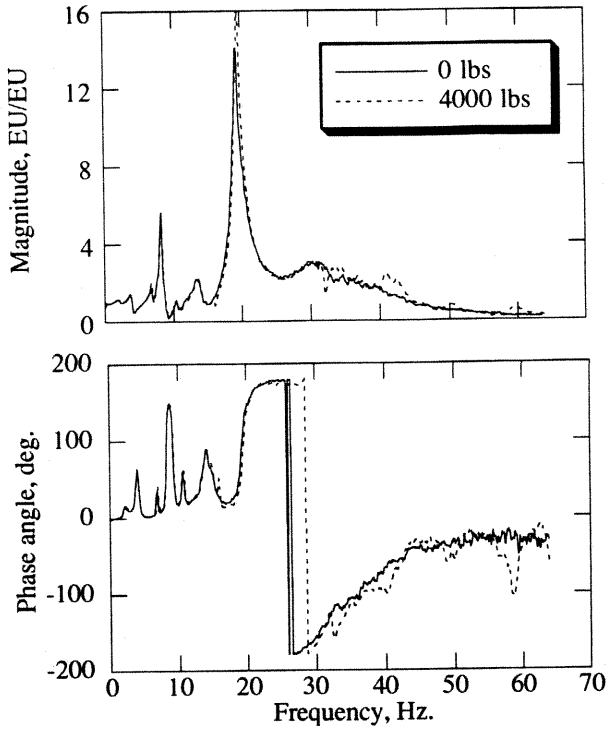


a. Axial force gage response

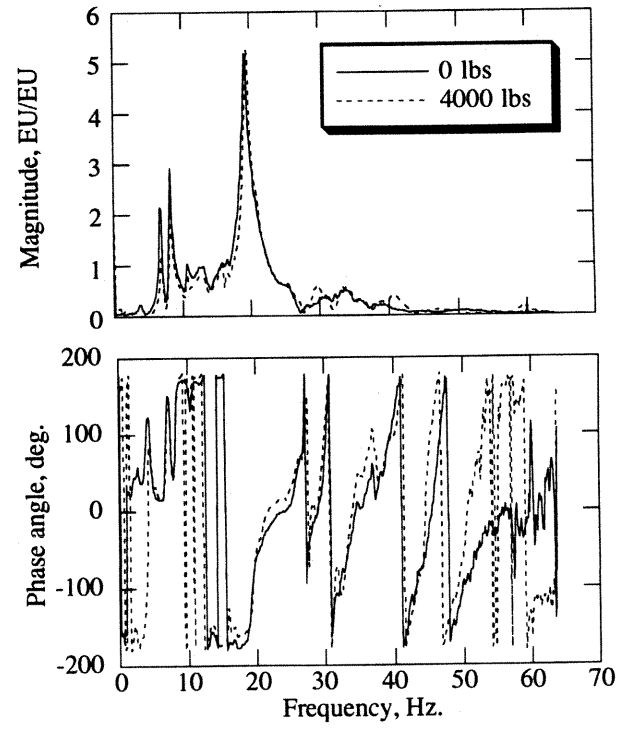


b. Normal force gage response

Fig. 8 Effect of rotor thrust on the balance response under hub axial force loading (no shaft rotation), simulated BO-105 hub mass.

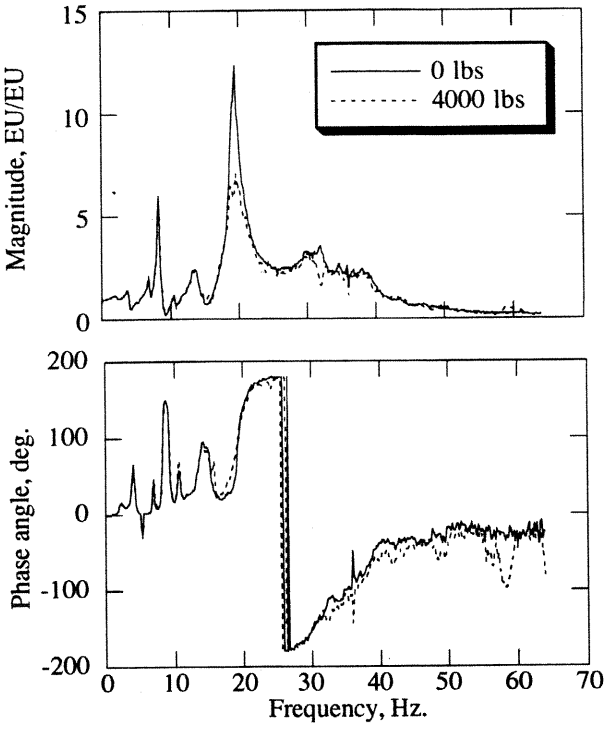


a. Axial force gage response

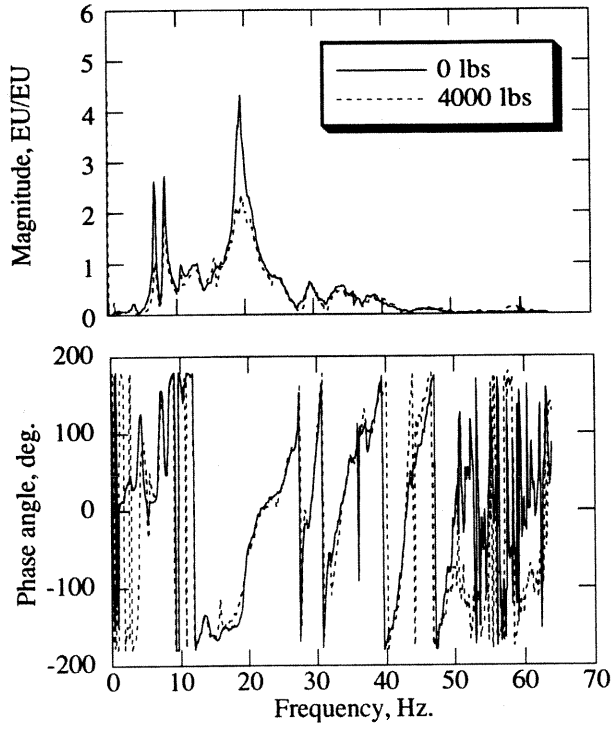


b. Normal force gage response

Fig. 9 Effect of rotor thrust on the balance response under hub axial force loading (shaft rotation =315 RPM), simulated BO-105 hub mass.

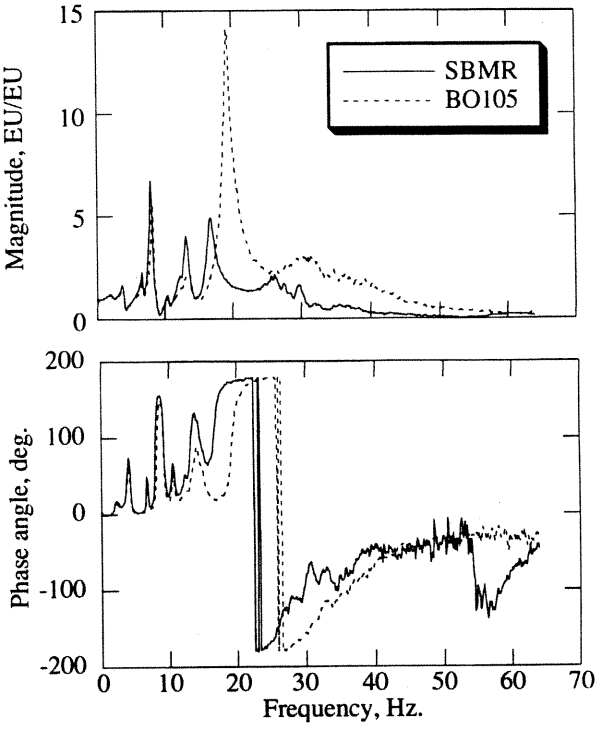


a. Axial force gage response

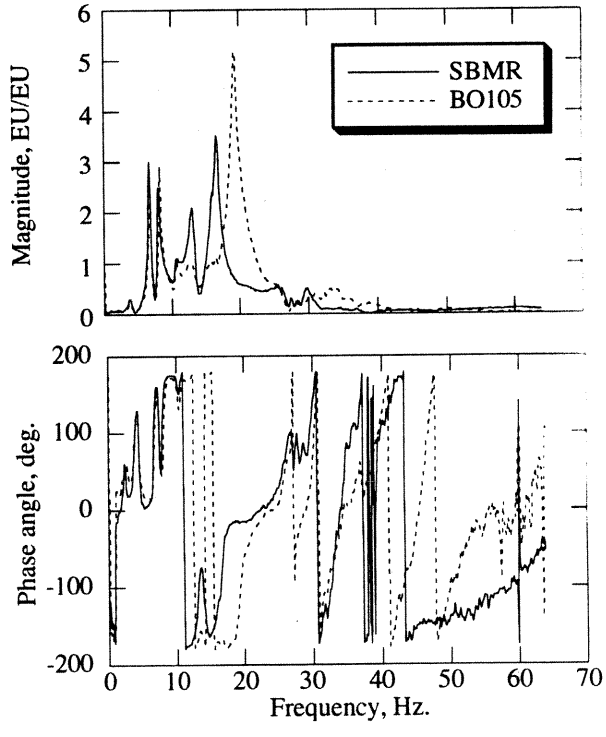


b. Normal force gage response

Fig. 10 Effect of hub mass on the balance response under hub axial force loading (zero shaft rotation and zero thrust preload).

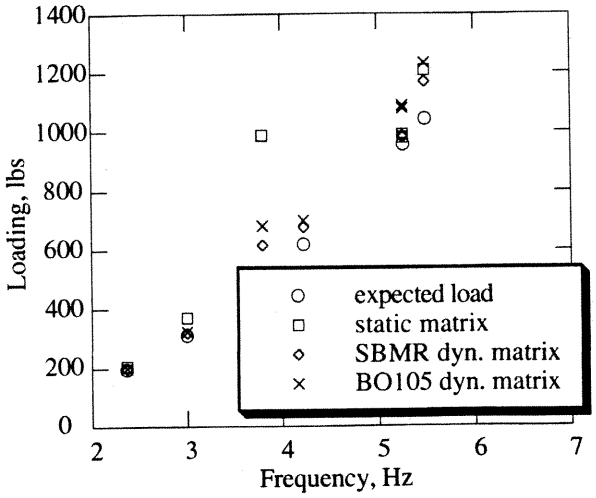


a. Axial force

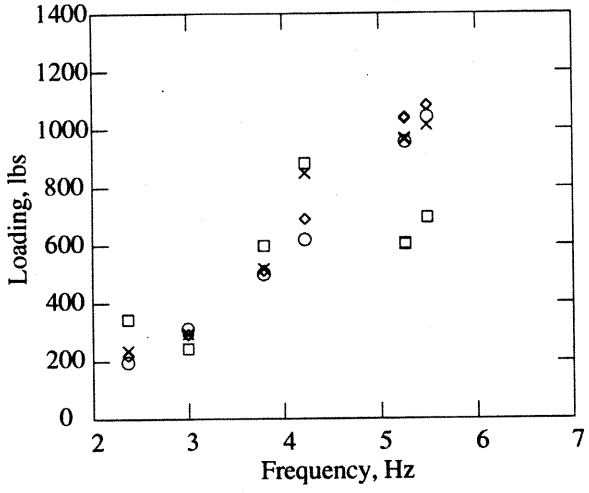


b. Side force

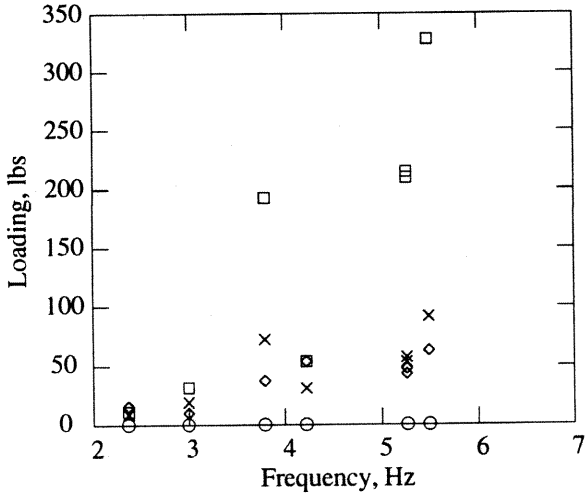


c. Normal force

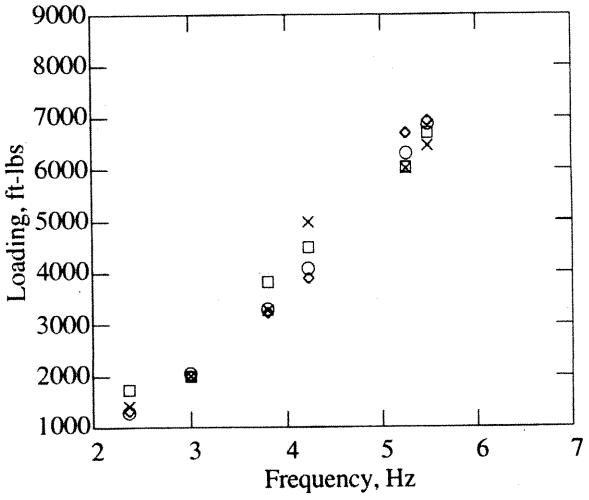


d. Roll moment

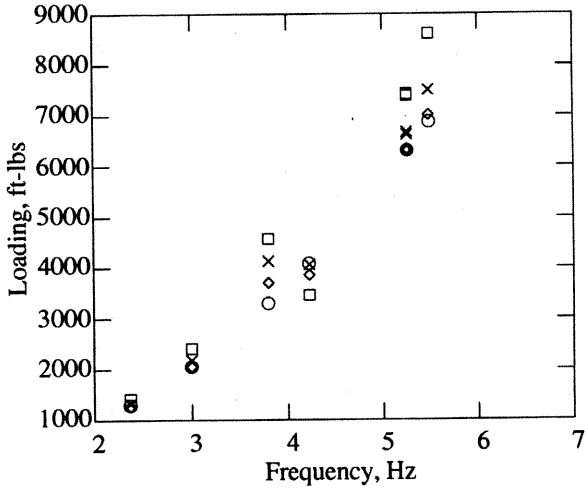


e. Pitch moment

Fig. 11 Prediction of balance 1/rev loading for the SBMR hub imbalance test using the static and dynamic calibration matrices.

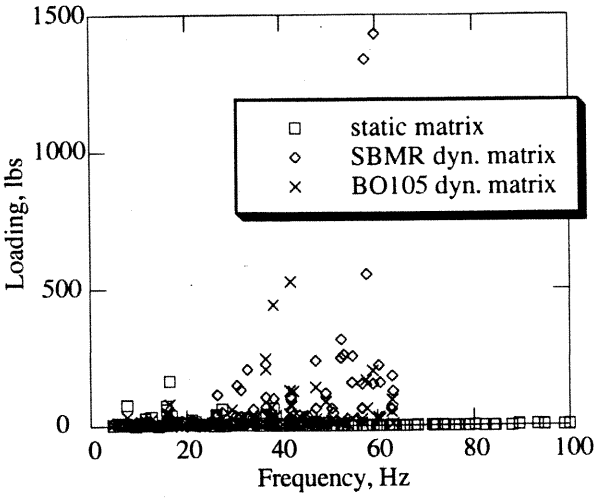


a. Axial force

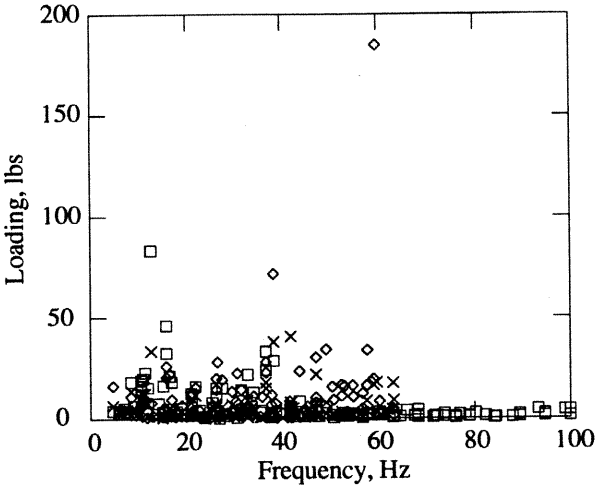


b. Side Force

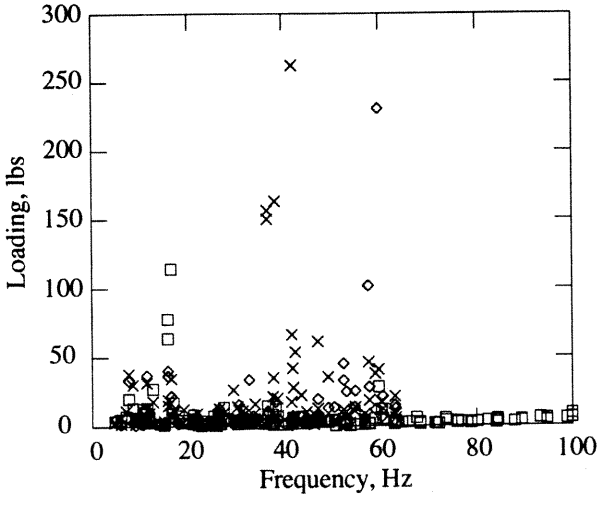


c. Normal force

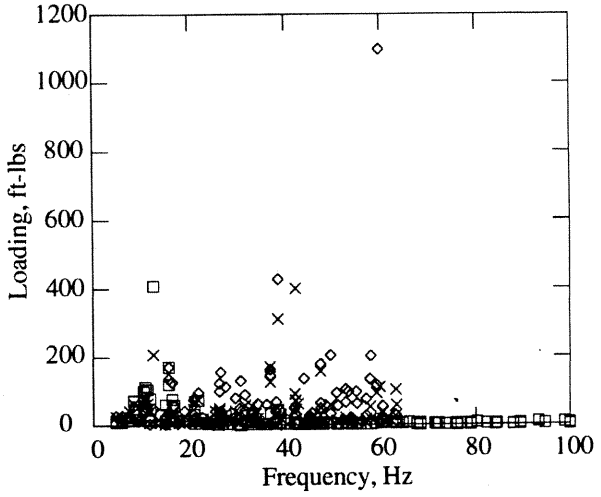


c. Roll moment

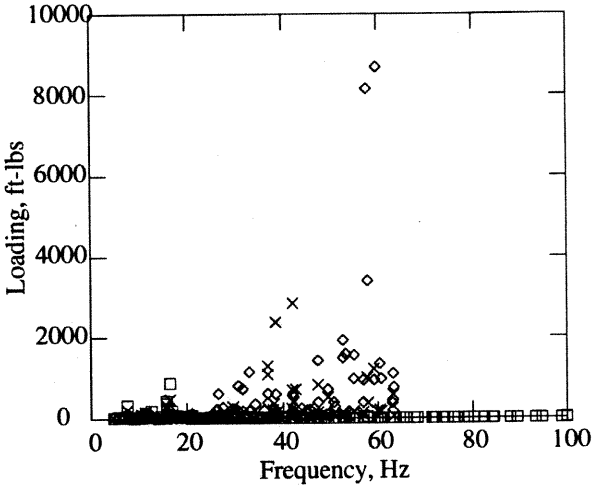


e. Pitch moment

Fig. 12 Prediction of balance n/rev harmonic loading, n>1, for the SBMR hub imbalance test using the static and dynamic calibration matrices

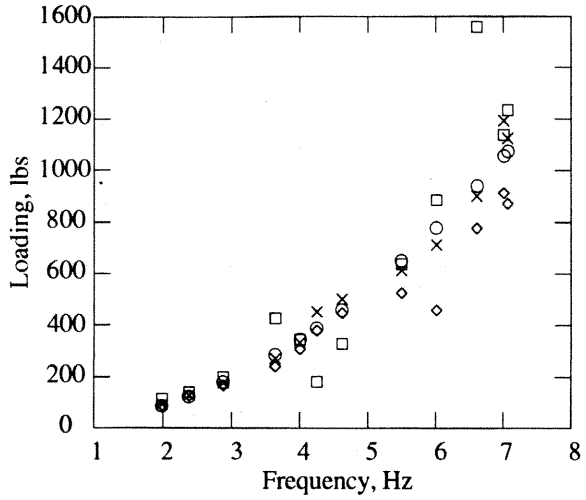


a. Axial force

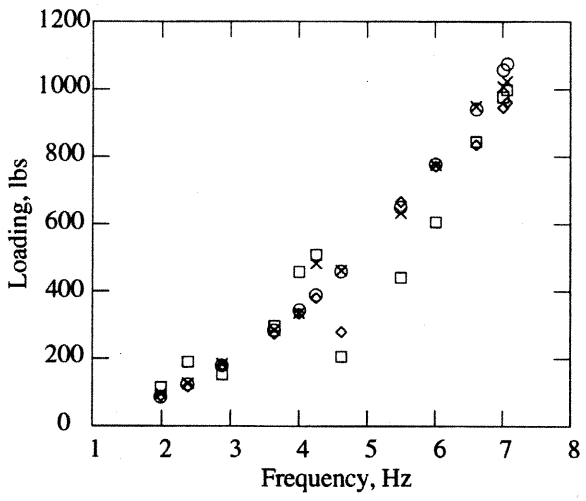


b. Side force

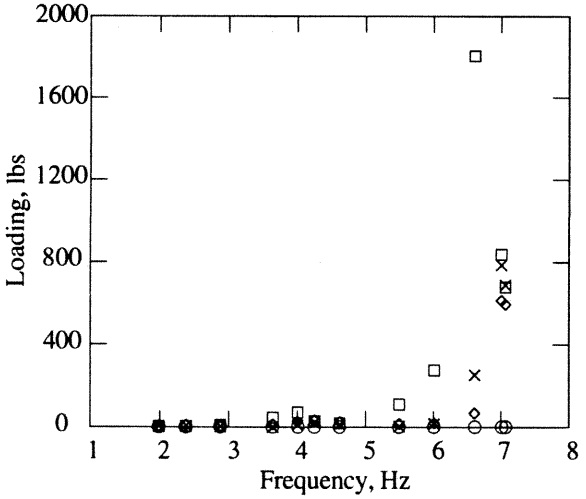


c. Normal force

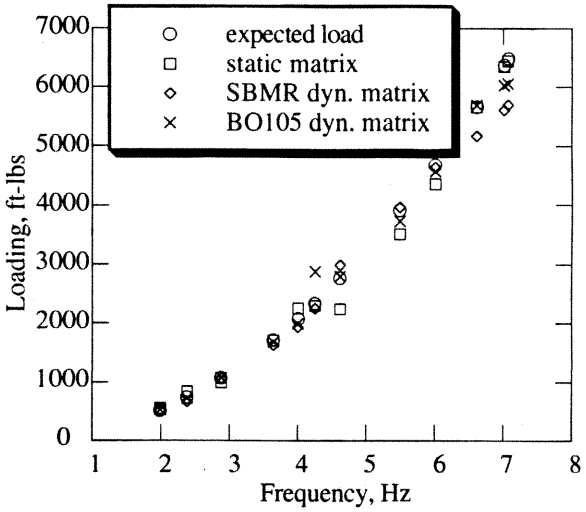


d. Roll moment

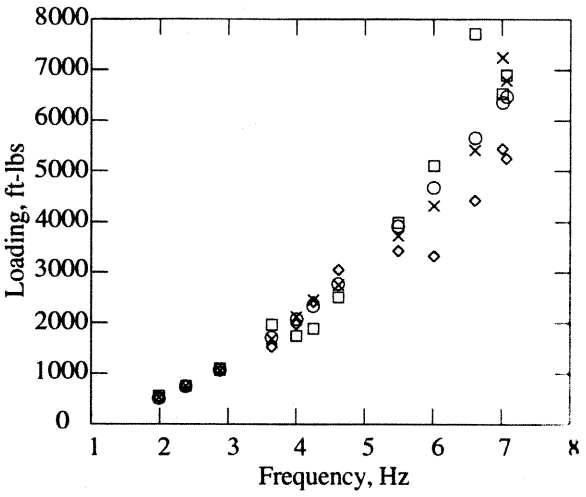


e. Pitch moment

Fig. 13 Prediction of balance 1/rev loading for the BO-105 hub imbalance test using the static and dynamic calibration matrices.

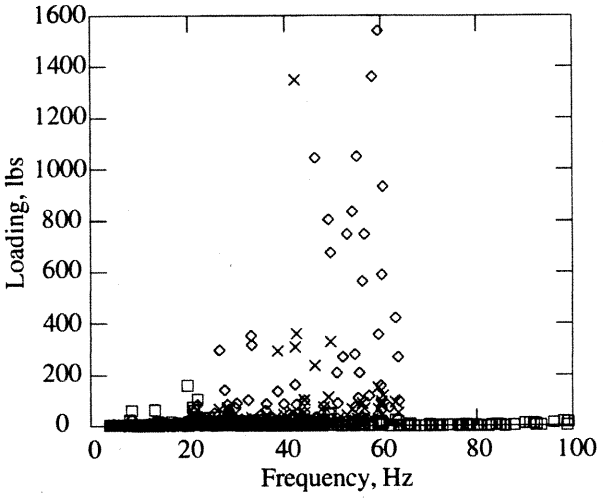


a. Axial force

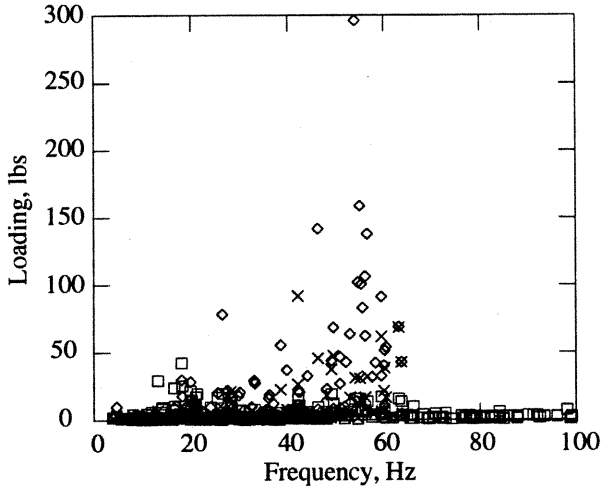


b. Side force

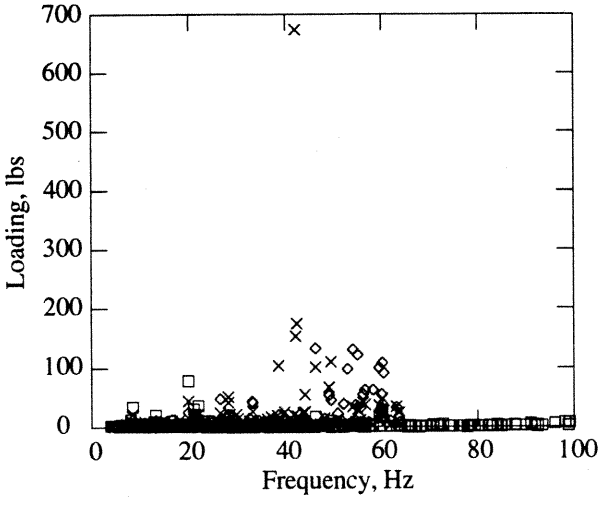


c. Normal force

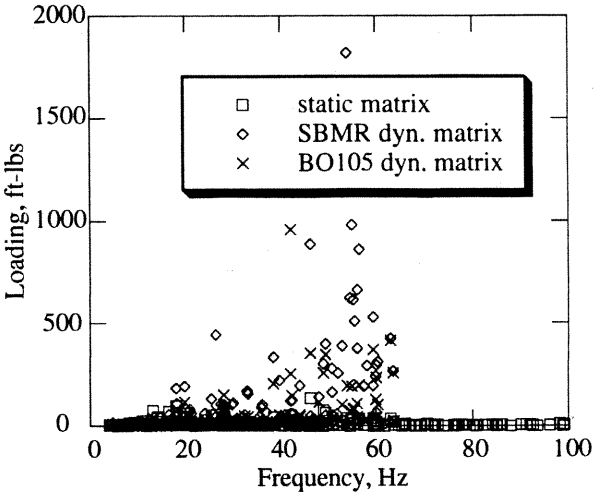


d. Roll moment

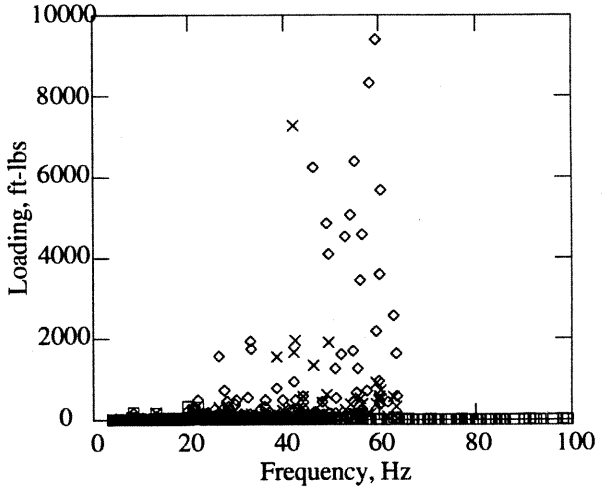


e. Pitch moment

Fig. 14: Prediction of balance n/rev harmonic loading, n>1, for the BO-105 hub imbalance test using the static and dynamic calibration matrices

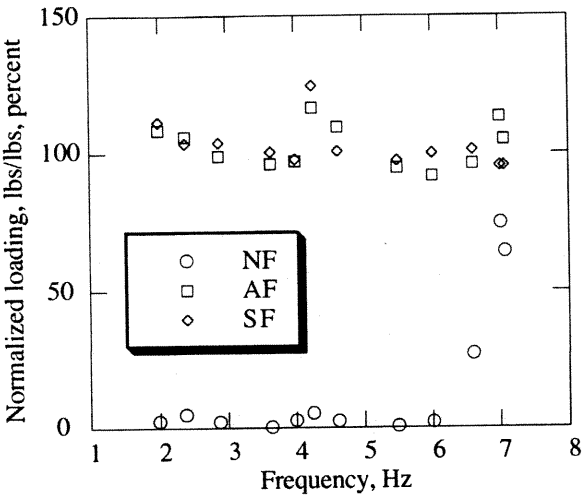


a. Forces

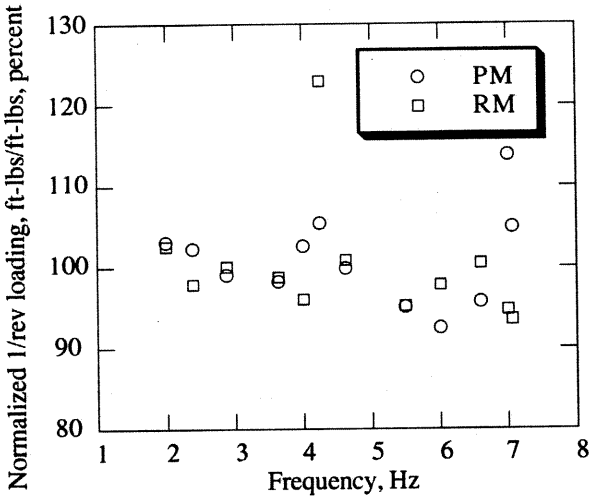


b. Moments

Fig. 15 Normalized balance 1/rev loading for the BO-105 hub imbalance test, calculated using the BO-105 dynamic calibration matrix.

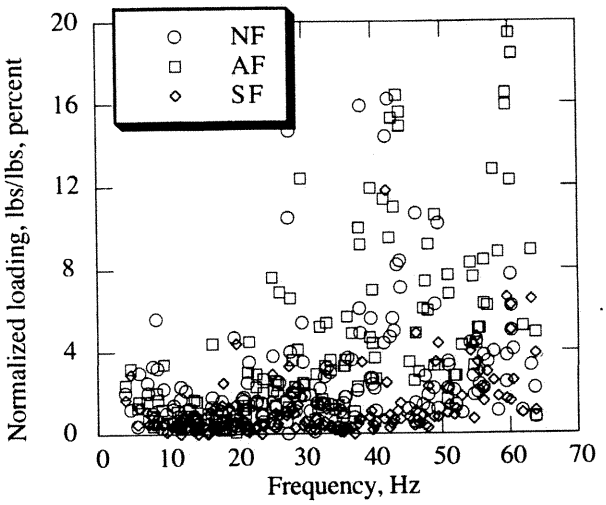


a. Forces

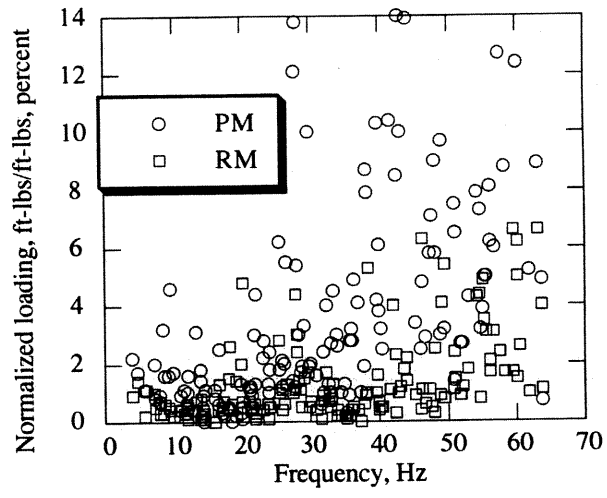


b. Moments

Fig. 16 Normalized balance n/rev loading, n>1, for the BO-105 hub imbalance test, calculated using the BO-105 dynamic calibration matrix.

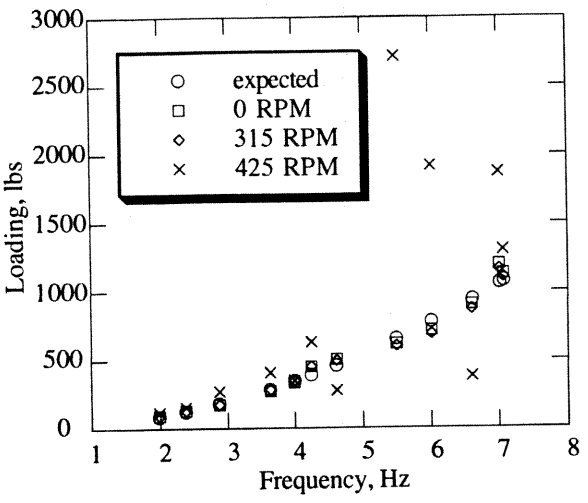


a. Axial force

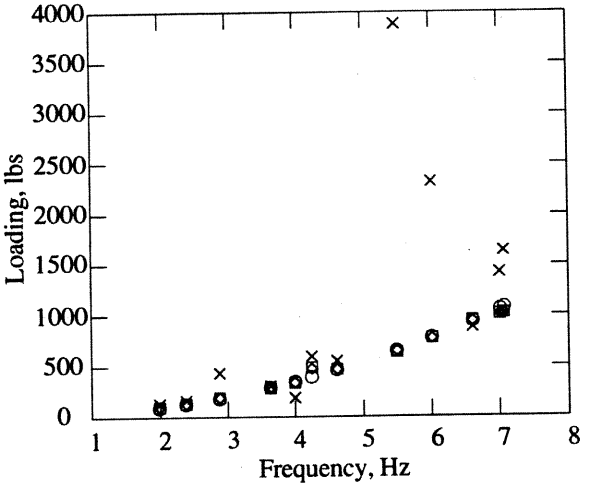


b. Side force

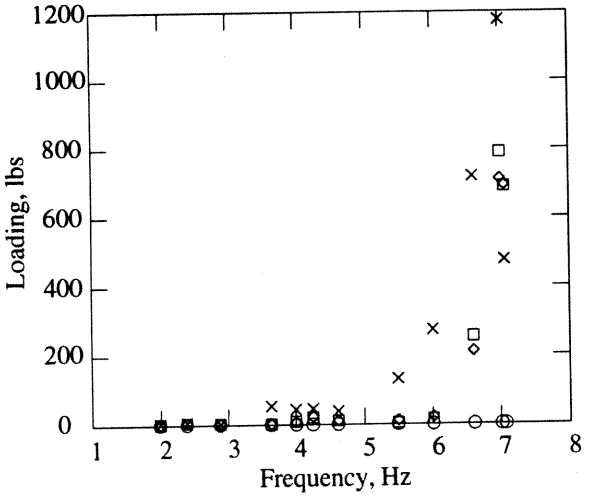


c. Normal force

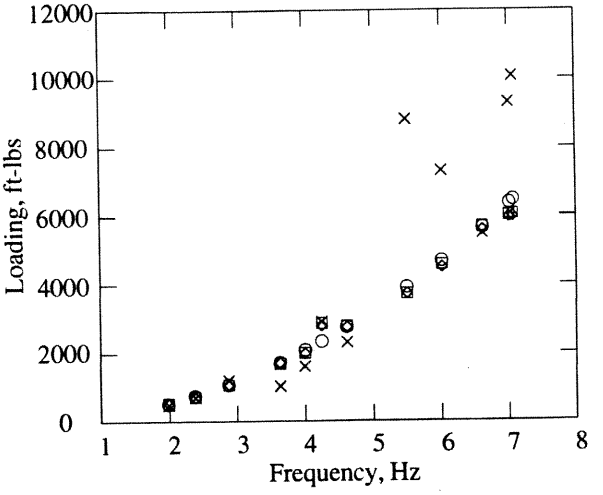


d. Roll moment

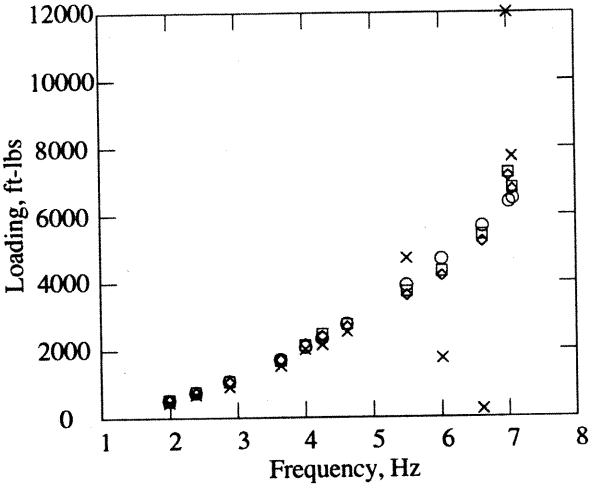


e. Pitch moment

Fig. 17: Prediction of balance 1/rev loading for the BO-105 hub imbalance test using the dynamic calibration matrices, based upon FRF data from the BO-105 shake test with and without shaft rotation.

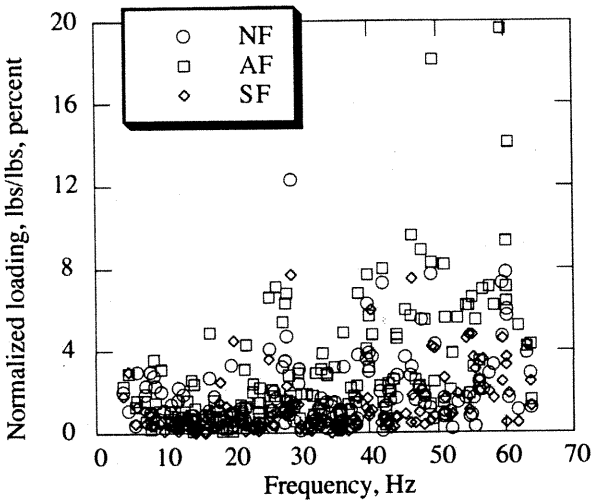


a. Forces

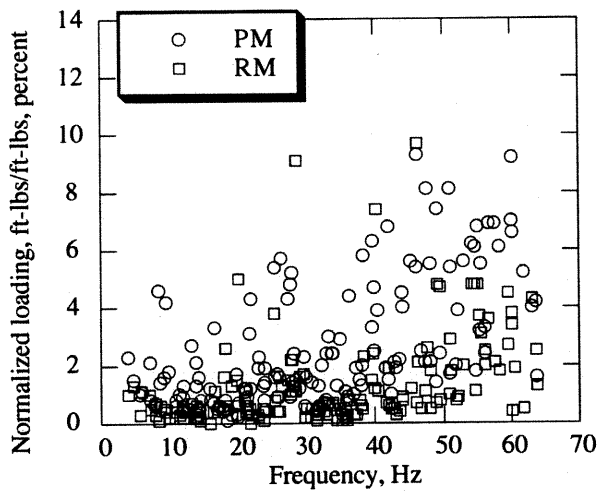


b. Moments

Fig. 18 Normalized balance n/rev harmonic loading, n>1, for the BO-105 hub imbalance test using the dynamic calibration matrix based upon FRF data from the BO-105 shake test with shaft rotation of 315 RPM.

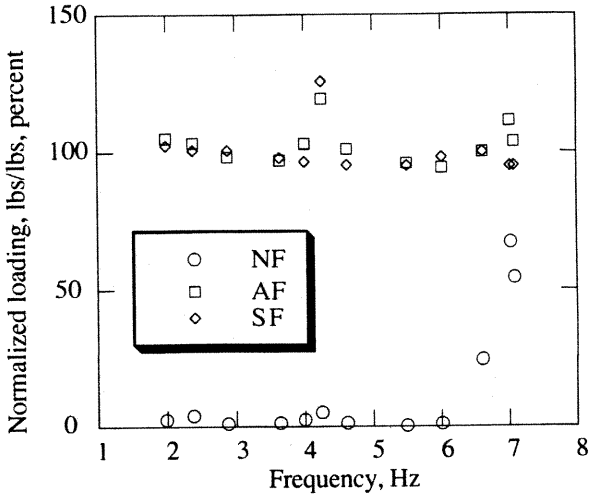


a. Forces

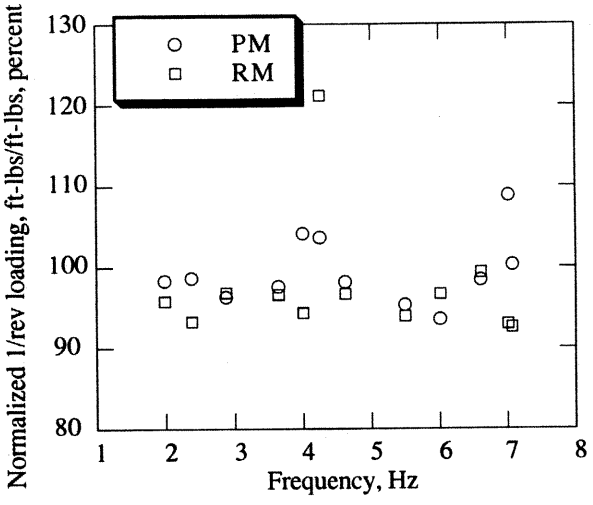


b. Moments

Fig. 19 Normalized balance 1/rev loading for the BO-105 hub imbalance test with the dynamic zero correction applied.

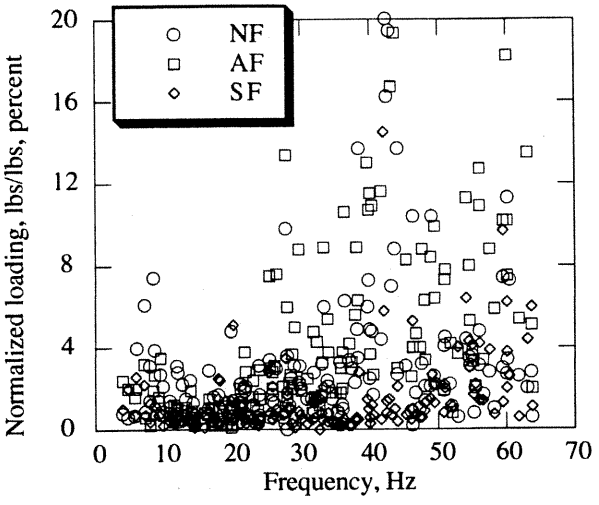


a. Forces

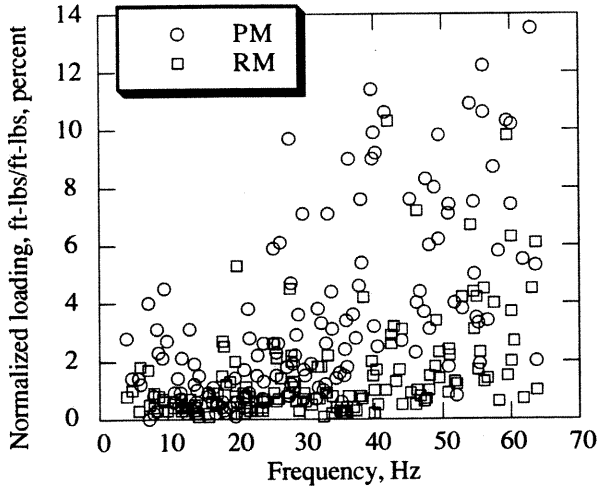


b. Moments

Fig. 20 Normalized balance n/rev loading, n>1, for the BO-105 hub imbalance test with the dynamic zero correction applied.

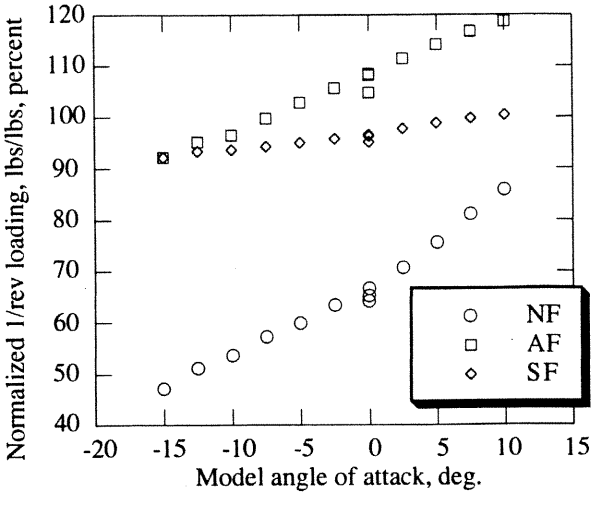


a. Forces

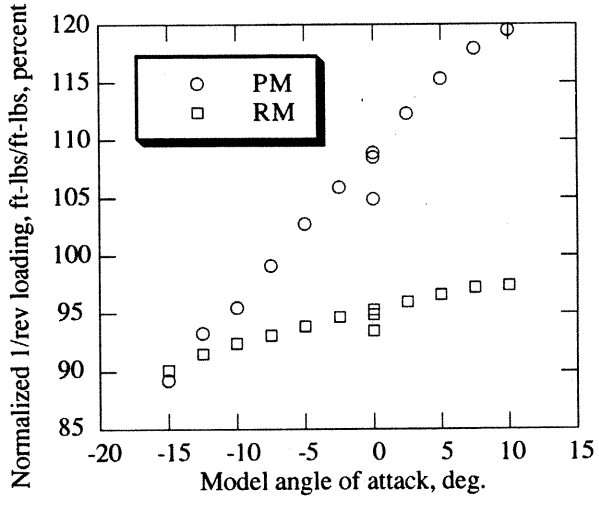


b. Moments

Fig. 21 Effect of angle of attack on the normalized balance 1/rev loading for the BO-105 hub imbalance test.